ASTROBIOLOGY
Volume 16, Number 4, 2016

DOI: 10.1089/ast.2015.1326

Mineralogy and Microbial Diversity of the Microbialites in the Hypersaline Storr's Lake, the Bahamas

Varun G. Paul,[1] David J. Wronkiewicz,[1] Melanie R. Mormile,[2] and Jamie S. Foster[3]

Abstract

Microbialites found in the low-light-intensity, hypersaline waters of Storr's Lake (SL), San Salvador Island, the Bahamas, were investigated with respect to their morphology, mineralogy, and microbial diversity. Previously described microbialite morphologies, as well as a newly identified ''multi-cuspate'' morphology, were observed at various depths. Electron microscopy analysis revealed the presence of angular, blocky, and needle-shaped crystals with mineralized cyanobacterial filaments and remains of exopolymeric substances. X-ray diffraction studies confirmed the presence of both Mg-calcite and aragonite in the plateau-mushroom and pinnacle mound microbialites, whereas only Mg-calcite was identified in the other microbialite morphotypes. A comprehensive molecular analysis using barcoded pyrosequencing of five different microbial mat communities identified at least 12 dominant bacterial phyla. Cyanobacteria were generally low in abundance and ranged from $\sim 0.01\%$ in the deeper pinnacle mounds to $\sim 3.2\%$ in the shallow calcareous knobs. Other photosynthetic members included green nonsulfur bacteria of the phylum Chloroflexi and purple sulfur bacteria of the class Gammaproteobacteria. All mat types contained significant amounts of sulfate-reducing and dehalogenating bacteria. The low light intensity reaching the deeper microbialites, the lack of dominant cyanobacteria, and the abundance of sulfate reducers and Chloroflexi collectively suggest that sulfate reduction and anoxygenic photosynthetic processes influence the carbonate biomineralization process in these systems. Key Words: Microbial mats—Microbial diversity—Biomineralization. Astrobiology 16, 282–300.

1. Introduction

Modern microbialites, such as stromatolites and thrombolites, are organo-sedimentary structures composed of lithified carbonate or siliceous material (Burne and Moore, 1987; Riding, 1991; Dupraz *et al.*, 2009). Microbialites represent one of the oldest ecosystems on Earth ($\sim$3.5 Ga; Hofmann *et al.*, 1999) and presently form in a wide range of habitats from coastal marine (*e.g.*, Reid *et al.*, 2000), hypersaline (*e.g.*, Skyring and Bauld, 1990; Glunk *et al.*, 2011), freshwater lakes (*e.g.*, Ferris *et al.*, 1997; Freytet and Verrecchia, 1998; Laval *et al.*, 2000), to deep-sea methane seeps (*e.g.*, Bailey *et al.*, 2009). Microbial mats, usually present on the surface of the microbialites, are considered to be the initiators and propagators of microbialite mineral structures and include a diverse microbial community involved in the trapping, binding, and precipitation of carbonate minerals. The microbial population, availability of sunlight, microbe-produced exopolymeric substances (EPS), wave/tidal energy in the environment, water depth, and the chemistry of the surrounding aqueous environment are some of the key factors that determine the growth and lithification potential of microbialites (Reid *et al.*, 2000; Riding, 2000; Dupraz *et al.*, 2004, 2006, 2013; Visscher and Stolz, 2005; Braissant *et al.*, 2007).

Microbial mats that have the propensity to form microbialite structures typically consist of six major functional guilds of microorganisms (Van Gemerden, 1993; Dupraz and Visscher, 2005) and include (i) oxygenic photoautotrophs, such as cyanobacteria that dominate the upper layers of the microbial mats; (ii) oxygenic heterotrophs that gain energy from the breakdown of organics; (iii) anoxygenic photoautotrophs that comprise purple and green bacteria; (iv) anaerobic heterotrophs, such as sulfate-reducing bacteria (SRB) capable of oxidizing organic material by coupling an electron transfer process with compounds like SO_4^{2-}; (v) sulfide-oxidizing bacteria that oxidize reduced sulfur compounds with O_2 or NO_3^- while fixing CO_2 into organic compounds; and (vi) fermenters, degrading organic carbon to generate energy along with SRB. Cycling of various organic and inorganic energy sources is important in the mat

[1]Department of Geological Sciences, Missouri University of Science and Technology, Rolla, Missouri.
[2]Department of Biological Sciences, Missouri University of Science and Technology, Rolla, Missouri.
[3]Department of Microbiology and Cell Science, University of Florida, Space Life Science Lab, Merritt Island, Florida.

ecosystem. For example, hydrogen production by cyanobacteria and consumption by members of Chloroflexi and SRB have been shown to be important metabolic processes in the functioning of a hypersaline mat community from Guerrero Negro, Mexico (Lee *et al.*, 2014).

Among the above-listed populations, the activity of oxygenic and anoxygenic phototrophs and SRB can result in the net precipitation of carbonate minerals (Visscher *et al.*, 2000; Dupraz and Visscher, 2005; Dupraz *et al.*, 2009). In modern stromatolites, oxygenic photosynthesis by cyanobacteria has been identified as the primary metabolism of the microbial mat community that leads to carbonate precipitation. In contrast, sulfide oxidizers and fermentative and aerobic heterotrophs will promote the dissolution of carbonate minerals (Dupraz and Visscher, 2005). The combined metabolic activities of the microbial mat communities coupled with the environmental conditions thus determine the net precipitation potential of the microbialites. Sulfur cycling between sulfate reducers and sulfide oxidizers has been evidenced to play a key role in the precipitation of carbonate minerals (Visscher *et al.*, 1998; Dupraz and Visscher, 2005; Breitbart *et al.*, 2009). Sulfate-reducing bacterial activity increases the alkalinity (HCO^{3-}) and thereby propagates carbonate precipitation, while the reactions involving sulfide oxidizers result in net dissolution (Visscher *et al.*, 1998). However, factors such as day-night cycle, presence/absence of oxygen, and the resulting complete or partial oxidation of HS^- further control the carbonate mineral precipitation potential due to the activity of these two groups of microorganisms (Dupraz and Visscher, 2005).

Phototrophic communities synthesize EPS, the production of which is directly influenced by light availability (Decho *et al.*, 2005). Precipitation and lithification are subsequently influenced through the decomposition of the EPS, which releases bound bicarbonate and calcium ions. In addition, favorable sites within the EPS matrix can serve as nucleation sites and templates for $CaCO_3$ precipitation (Dupraz and Visscher, 2005). Not all microbial mats, however, undergo mineral precipitation and lithification. For example, the hypersaline mat communities of Guerrero Negro, Mexico, harbor many of the same functional guilds of microbes found in microbialites yet do not undergo lithification (Ley *et al.*, 2006).

The mineralogy constituting modern microbialites can vary from carbonate minerals, such as Mg-calcite, and aragonite (Neumann *et al.*, 1989; Reid *et al.*, 2000), to siliceous deposits (Jones *et al.*, 1998), while fossil microbialites also contain chert and dolomite due to diagenetic changes (Sommers *et al.*, 2000). Dolomite has been shown to form diagenetically in microbial mats, especially along anoxic sediment layers (Furman *et al.*, 1993; Vasconcelos and McKenzie, 1997).

Storr's Lake (SL), located on the eastern portion of San Salvador Island, the Bahamas (Fig. 1), formed during the late Holocene sea level rise, when a depression on the east side of the island was flooded and subsequent evaporitic conditions caused the lake to become seasonally hypersaline (Neumann *et al.*, 1989; Zabielski, 1991). The lake is shallow, with a maximum depth of <2 m (Mann and Nelson, 1989), and is slightly alkaline and extremely turbid. The salinity of the lake water generally fluctuates depending on evaporation rates and the frequency of rain. The turbidity in the lake is caused by floating planktonic material and benthic components that become suspended after they trap gas bubbles released from microbial metabolism (Mann and Nelson, 1989; Neumann *et al.*, 1989). Storr's Lake is an unusual system due to the growth of microbialites in shallow water, in spite of the limited light conditions caused by high turbidity.

Four distinct microbialite morphologies in SL have been previously identified in discreet zones (Mann and Nelson, 1989; Neumann *et al.*, 1989). Moving along a transect from western shore to the lake center, the first morphotype is clotted thrombolitic pie mounds. These are located in shallow water and periodically undergo desiccation during dry periods with low lake levels when they are subaerially exposed. As the lake continues to deepen, there is a point where the bottom exhibits a slight elevation and calcareous knobs begin to appear (the ''bulbous crust'' of Neumann *et al.*, 1989). The upper parts of the $\sim$15 cm calcareous knobs may also be subaerially exposed during periods of low water level. Continuing farther into the lake, the water

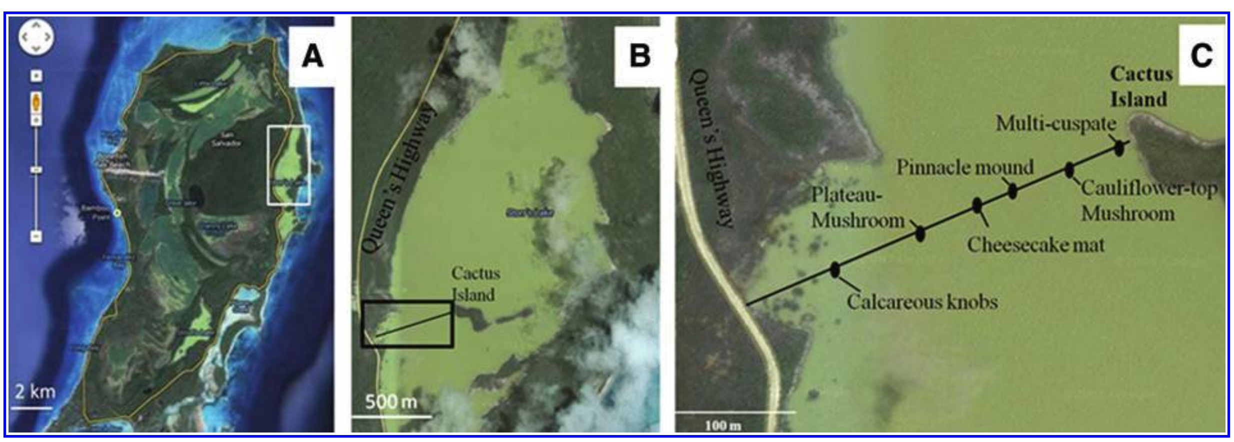

FIG. 1. Overview of the collection sites at SL. (**A**) Google map of San Salvador Island with SL located along the eastern margin of the island (white box). Bar = 2 km. (**B**) Magnified image of white box region depicting the northern section of SL. The line indicated within the black box represents the approximate transect along which the water and microbialite samples were collected. Bar = 500 m. (**C**) Magnified Google map image of the black box in (B) showing the locations where the different microbialites and microbial mats were sampled in 2011 and 2012.

depth increases, and flat-topped plateau stromatolites with hard calcified structures firmly attached to the carbonate substrate of the Pleistocene Cockburn sequence are observed at 10–15 cm below the water surface. In the deepest locations of the lake, the club-shaped, columnar, pinnacle mounds, which extend up to 70 cm in length, are found. Note that the water level varied between the different studies. In addition to the hard-calcareous microbialites, there are three nonlithified to weakly lithified microbial mat types that have been profiled in the lake: (i) near-shore ectoplasmic pie mounds, (ii) an offshore mat that covered the calcareous knobs, and (iii) a thick, leathery, ''cheesecake'' microbial mat present in between, and on top of, the deeper microbialites (Neumann *et al.*, 1989). The deeper, larger microbialites have been suggested to be covered all year long under the bottom gelatinous sediments and may have become, or are becoming, inactive (termed a ''sub-fossil''), and some of them exhibit features of diagenetic alteration (Dupraz *et al.*, 2006, 2013; Fowler, 2011). Submerged mats in SL exhibit a low rate of photosynthesis and nitrogen fixation relative to open marine microbialites (Paerl *et al.*, 2003; Dupraz *et al.*, 2013).

Previous morphological studies of the microbial population in SL have identified several taxa within the different mats found in the lake bottom and the shallow calcareous knob microbialites, including cyanobacteria, such as *Scytonema, Gloeocapsa, Schizothrix, Phormidium, Microcoleus, Calothrix, Spirulina,* colorless sulfur bacteria *Beggiatoa,* purple sulfur bacteria *Chromatium,* and so on, and diatoms like *Navicula* and *Nitzschia* (Mann and Nelson, 1989; Neumann *et al.*, 1989; Pentecost, 1989). A 16S rRNA gene analysis of the microbial population of the near-shore calcareous knob also identified at least five genera of SRB including *Desulfovibrio, Desulfobulbus, Desulfococcus, Desulfobacter,* and *Desulfobacterium* (Brigmon *et al.*, 2006). The Brigmon study also indicated that the cyanobacteria were reported to be dead in the evaporitic mats present in the nonphotic zone of SL, whereas nonphotosynthetic bacteria were dominant in these regions.

Most modern microbialites studied to date (Burne and Moore, 1987; Reid *et al.*, 2000; Visscher *et al.*, 2000), with the notable exception of deep-sea occurrences (Bailey *et al.*, 2009) and those at Pavilion Lake (Laval *et al.*, 2000; Lim *et al.*, 2009), are located in shallow, clear-water environments. Identification of microbialites in locations such as SL has broadened our understanding of the range of aquatic habitats, where these organo-sedimentary structures have developed throughout recent and ancient Earth history. The high-turbidity waters of SL limit sunlight availability, especially to the deeper-water microbialites, and thus likely impede the development of their phototrophic population. The lake water with a low visibility of approximately 10 cm further hinders any assessment of the spatial extent of the various microbial morphotypes. Determining the light availability at different depths, the water chemistry, and the microbial mat composition is critical to understanding the complex role of the various biogeochemical components on the development of the microbialites. Although several previous studies have examined the microbialites in this lake environment, there has been no comprehensive analysis of the diversity in the different types of microbial mats associated with the microbialites. In this study, we applied 16S rRNA gene sequencing to assess the microbial diversity of the surface mats associated with both the shallow and deeper microbialites. Additionally, we describe a new morphotype of microbialite, the ''multi-cuspate'' type, which was discovered in the lake; and we present new results of our investigations on several of the lake properties including the water chemistry, the intensity of sunlight penetrating into the water, and the mineralogy of the microbialites. The overall goal of this study was to build upon previous studies on SL to enhance our understanding of the biogeochemical processes that influence the characteristics of the water, and the mineralogy and microbial mats associated with hypersaline microbialites.

2. Materials and Methodology

2.1. Site description and sample collection

Samples were collected from SL, San Salvador Island of the Bahamas, along a roughly east-west transect along the western shore during three visits in April 2011, June 2012, and June 2013 (Fig. 1). Year 2011 was relatively dry for San Salvador Island, with the total rainfall for the months of February and March recorded at only $\sim$1.0 cm. In 2012 and 2013, the lake received a substantial increase in the amount of freshwater inflow due to heavy seasonal rains. The total rainfall recorded for the combined months of May and June 2012 and 2013 were $\sim$34.0 and $\sim$22.2 cm, respectively (source: http://www.accuweather.com/en/bs/the-bahamas-weather). The inflow of brackish water near our sampling location is funneled through a conduit running beneath the roadway (Fig. 2A) that connects SL to the small ephemeral ponds lying to the west of the road. The inflow of brackish water from the west causes the lake to exhibit two visually different zones: a relatively clear, brown tannin-colored and lower-salinity zone closer to the western shore, and a turbid, high-salinity zone farther into the lake (Fig. 2B). The mixing zone between the two water types moves farther from shore following periods of high rainfall and runoff. The high-turbidity and high-salinity water exhibits a characteristic reddish-brown color that is commonly observed in many other lakes in the Bahamian Islands and other marginal marine systems (Figs. 1A and 2C).

The water depth relative to the microbialites was measured with a centimeter-marked PVC pipe at random locations along a transect. The length between the top surface of the lake sediments and the water surface was noted as the water depth. The transect was started near a human-made conduit inlet to the lake on the western shore to Cactus Island in the northern portion of the lake (Fig. 1B). Our sampling transect was similar to that of Mann and Nelson (1989, section B-B') and Neumann *et al.* (1989). Water samples ($\sim$20–50 mL) were collected at different locations along the transect, and several water depth sample profiles were also collected. For comparison purposes, ocean water was also collected in 2012, directly south of SL, from Dim Bay. Microbialite and water samples were collected in 2011 and 2012, and only water samples were collected in 2013. Five different microbialites were identified and sampled: calcareous knobs, plateau-mushroom, pinnacle mound, cauliflower-top mushroom, and a newly identified type, ''multi-cuspate.'' The microbial mats found on the surface of the microbialites ranged in thickness from a few millimeters to $\sim$1 cm and were uniform to sporadic in their distribution on the surface. The offshore ''cheesecake''

FIG. 2. (**A**) The conduit located on the western shore of SL through which the brackish meteoric runoff water entered the lake. (**B**) Image of the lake from the western shore in 2013 showing the mixing zone between the two different water turbidity zones with the transition shown by arrows. Distance from shore to the transition zone is ~ 60 m. Cactus Island forms the shoreline in the background in right half of photograph. (**C**) Image taken in 2011 of a calcareous knob microbialite with its head sticking out of the reddish-brown lake water.

leathery mats, first described by Neumann *et al.* (1989), were ubiquitous across deeper portions of the lake bottom and were previously suggested to envelop the surface of microbialite heads at the deeper locations. Though this was true in some cases, we observed that the heads generally rose above the sediment surface and were covered by a microbial mat that was thinner than the leathery mats. Microbial mat samples were collected from the top surfaces of the four microbialite morphotypes, as well as the offshore, leathery ''cheesecake'' mat in April 2011 and June 2012. The surface of the shallow-water calcareous knob microbialites had occasional eukaryotic algal material growing over them, but the algae were avoided during sampling as much as possible. Replicate mat samples were aseptically collected (5–10 g each) and immediately stored in a nucleic acid preservation solution (LifeGuard Soil Preservation solution, MoBio Laboratories, Carlsbad, CA, USA). The mat samples were transported back to the Gerace Research Centre (GRC) lab on San Salvador Island and placed in a freezer within 8 h of sampling. They were then transported to the Missouri University of Science and Technology (Missouri S&T), where the mats were stored at −20°C until processed.

2.2. Characterization of Storr's Lake water

The water samples were analyzed on site and at the laboratory in GRC, or they were transported to Missouri S&T for further laboratory analysis. *In situ* water measurements included pH and redox potential (Accumet AP115 portable pH meter, Fisher, Pittsburgh, PA, USA), light intensity (described below), conductivity, temperature (WTW Cond 333i, Weilheim, Germany), and dissolved oxygen (Accumet AP64, Fisher Scientific, Houston, TX, USA). Alkalinity, Ca, and total hardness measurements were performed by colorimetric titration (HACH, Loveland, CO, USA). Water samples for alkalinity measurements were filled up completely in a 1 L Nalgene bottle, capped tightly, and shielded from sunlight to prevent heating. Measurements of alkalinity were performed anywhere within 1 (on shore) to 6 h (at GRC) after sample collection. Samples were diluted 1:100 with deionized water before testing for their Ca-Mg hardness values. The water samples for cation and anion analysis were filtered on site with disposable 0.45 μm cellulose acetate syringe filters and later returned to the Missouri S&T laboratory. Major element cations (Ca, Mg, Si, K, Na, Fe, Mn, and Al) were analyzed with a Perkin-Elmer Optima 2000 DV inductively coupled plasma–optical emission spectrometer at Missouri S&T, and anions were analyzed with a Dionex DX-120 ion chromatography unit at VHG Labs (Manchester, NH). Analysis of standards before, during, and after measurements indicated an accuracy of better than ±0.05 pH units for the 7.0 pH standard (*i.e.*, ±0.7% error on a log pH scale) and a precision better than 99.8%. An average error percentage of ±8.2% and ±3.2% was calculated for the conductivity probe when checked with 1008 and 100.8 mS/cm standards, with precisions better than 95.5% and 92.1%, respectively. For the inductively coupled plasma–optical emission spectrometry (ICP-OES) analysis, commercially traceable standard solutions were used for calibration and for quality control checks during each run. Using the standard checks, we observed the overall average accuracy with the ICP-OES analysis to be within ±5.0% error range for 1.0 ppm and ±6.0% for 10 ppm standards. Precision values, reported as relative standard deviation obtained between duplicate measurements of randomly chosen samples, ranged from ±97.0% for most elements, while Na, Al, Si in certain samples had a precision better than ±90.0%. The PHREEQ software program was used to calculate saturation index (SI) values in SL water (Saini-Eidukat and Yahin, 1999).

Turbidity and light penetration depths were qualitatively evaluated during the 2012 and 2013 sampling trips with an underwater video camera and quantitatively *ex situ* with a HACH nephelometric turbidity units (NTU) light-scattering device, or *in situ* with a Secchi disk, and light intensity loggers from HOBO (Cape Cod, MA, USA). The waterproof HOBO light meters were placed at several locations at the bottom of the lake, and the data were recorded with the HOBOware program. The HOBO probes were attached to metal spikes by using monofilament thread and anchored into the bottom sediment of SL adjacent to the microbialite mounds. The probes were also attached to floating fishing bobbers to allow the units to be relocated and recovered. To determine the long-term settling rate of the particles in the lake water, the turbidity of water was measured at regular intervals under controlled, enclosed conditions. The water sample collected in 2012 was taken in a clean glass vial and allowed to remain in the HACH NTU light-scattering device for a 6-month period at room temperature, as turbidity values were measured. A comparison was also made to illite (illite-bearing shale, Fithian, Illinois) and smectite clay (Wards Scientific and Clay Mineral Society Standard, STX-1) samples suspended separately into a 5% synthetic seawater solution.

2.3. Mineralogy and microscopy of the microbialites

The X-ray diffraction (XRD) technique was employed to determine the mineralogy of the microbialites. The first set of analyses included homogenized microbialite samples collected from $\sim 1\,cm^3$ partitioned replicate sections from random positions within each of the five microbialite heads, including the walls, nodes, and highly compacted bottom layer. These sections were used to provide an overall average composite sample for each microbialite. The microbialites that displayed peaks for both Mg-calcite and aragonite were characterized in more detail both vertically and laterally by collecting individual samples from carefully partitioned $\sim 2\,cm^3$ regions at different positions throughout half-sectioned microbialite mounds. All samples were hand crushed to a powdery consistency with an agate mortar and pestle, rinsed three times with deionized water to remove soluble salts and low-density organic particles, and then dried in the oven at 55°C overnight. Samples were scanned between 6° and 90° 2-theta at a scan rate of 2.8° (2-theta) per minute using a PANalytical X'Pert Pro multipurpose X-ray diffractometer (PANalytical, Netherlands) with a CuKα radiation source.

High-precision elemental analysis was performed on acid-digested samples of the pinnacle mound and plateau-mushroom microbialites by ICP-OES. The digestions were performed on identical sample splits from the second set of individual XRD analysis samples. Approximately 0.25 g of each sample was rinsed with deionized water, dried overnight in an oven at 55°C, weighed to 0.01 g accuracy, and then digested in a 10 mL volume solution of 5% high-purity Ultrex HNO_3. The digested solution was filtered through a 0.45 μm cellulose acetate syringe filter; then major and minor element cations (Ca, Mg, and Sr) were determined by the Perkin Elmer Optima 2000 DV ICP-OES system. The accuracy of the analysis with respect to solutions of the respective standards is discussed earlier for all elements.

Scanning electron microscopy–energy dispersive spectroscopy (SEM-EDS) analytical techniques were used to provide a semiquantitative elemental composition and spatial-morphological analysis of the crystals present in the solid microbialites. Samples were sputter coated with Au/Pd for 2 min to prevent charging and then were analyzed by a Hitachi S4700 SEM-EDS system. A rhombohedral grain of hydrothermal vein calcite was used as a positive control standard for SEM-EDS analysis. The plateau-mushroom microbialite was subjected to two additional analyses: (i) a reflected light microscopic analysis conducted on thick, epoxy-coated cuttings of the top 2 cm calcified portion of the microbialite to identify the association and characteristics of the grains and (ii) an optical microscopic analysis of the microbial mat present on the surface of the microbialite to study the relationship between the microorganisms and minerals.

2.4. DNA extraction and 16S rRNA gene analysis

To determine the composition of the microbial mat community in SL, a 16S rRNA–based gene analysis by using multiplex barcoded pyrosequencing method was performed. Genomic DNA (UltraClean Soil DNA Isolation Kit, MoBio Laboratories, Carlsbad, CA, USA) was extracted in triplicate from microbial mats associated with the calcareous knobs, plateau-mushroom, cauliflower-top mushroom, and pinnacle mound microbialites, as well as a nonlithifying cheesecake microbial mat. The extracted DNA was sent to MoGene, LC (St. Louis, MO, USA) for 16S rRNA gene amplification and sequencing. Amplicon libraries were generated by using barcoded primers that target the V1–V3 region of the 16S rRNA gene. The bacterial primers used were 27-Forward AGRGTTTGATCMTGGCTCAG (Weisburg *et al.*, 1991) and 518-Reverse CGTATTACCGCGGCTGCTGG (Muyzer *et al.*, 1993). The primers incorporated the Titanium Lib-A adaptor and barcode sequences specific for the individual samples (Supplementary Table S1; Supplementary Information is available online at www.liebertonline.com/ast).

The polymerase chain reaction (PCR) mixture included 1X Master mix (MOLZYM Mastermix 16S Basic, Molzym, Bremen, Germany), 0.2 μM each of the barcoded forward and reverse primers, 0.51 U Taq DNA polymerase (MolTaq, Molzym), 30 ng of the template DNA, and DNA-free water for a final volume of 25 μL. Conditions for PCR were 96°C for 5 min, 25 cycles of 95°C for 10 s, 56°C for 30 s, and 72°C for 30 s, followed by a single cycle of 72°C for 5 min. The amplicon libraries were normalized, pooled, and then pyrosequenced with Titanium chemistry (454 GS-FLX, Roche, Branford, CT, USA).

The bioinformatics software program QIIME was used for processing, cluster analysis, and classification of the raw sequences (Caporaso *et al.*, 2010). High-quality reads were separated based on the barcode sequences and analyzed for phylogenetic origin by comparison to reference database Greengenes (DeSantis *et al.*, 2006). The ChimerSlayer program available in QIIME was used to perform a Chimera check (Haas *et al.*, 2011). Community analysis and comparison of the mat types were performed phylogenetically by using Unifrac jackknifed environmental clustering that compares distances between communities (Lozupone and Knight, 2005). QIIME was also used to calculate the alpha diversity index parameters, such as Chao1, Shannon, and observed species. The program randomly generated a subset of sequences (termed ''equalized''), and 10 iterations were run for each diversity indices. The sequencing reads obtained from SL were submitted to NCBI Sequence Read Archive (SRA) with accession number SRP031628. Note that the sequences obtained from plateau-mushroom mats were submitted as ''plateau,'' and the cauliflower-top mushroom mat sequences were submitted as ''mushroom.''

3. Results

3.1. Water chemistry analysis

A water chemistry profile was generated throughout the SL transect at different depths and locations. Table 1 provides the average values for the various parameters measured in the lake over 3 years. The maximum water depth from the bottom sediment to the surface increased from 1.0 m in April 2011 to 1.1 and 1.3 m in June 2012 and June 2013, respectively. Mann and Nelson (1989) reported that depths < 2.0 m were observed in the lake, although these maximum depths were likely observed in other portions of the lake that were not transected during our field visits. Water

Table 1. Water Parameters Measured during the Three Sampling Years

Parameters	*March 31–April 01, 2011 15:00 (EST)*	*June 16–20, 2012 15:00 (EST)*	*May 30–June 3, 2013 16:00 (EST)*	*Seawater June 16, 2012 14:00 (EST)*
Max. water depth	~1 m	~1.1 m	~1.3 m	–
pH	8.22 (±0.05)	8.58 (±0.08)	8.22 (±0.20)	8.26
Eh (mV)	–60 (±2)	–80 (±12)	–73 (±14)	–55
Alkalinity (mg/L as $CaCO_3$)	178 (±8)	151 (±1)	140 (±27)	113
Ca hardness (mg/L as $CaCO_3$)	–	1,328 (±40)	1,150 (±233)	1,060
Mg hardness (mg/L as $CaCO_3$)	–	6,953 (±296)	6,340 (±466)	5,840
Temperature (°C)	27.5 (±1.0)	28.7 (±1.2)	24.6 (±0.2)	28
Conductivity (mS/cm)	138 (±4.5)	64 (±1.3)	59 (±2.3)	53.9
Salinity (ppt)	92.1 (±3.0)	42.7 (±0.9)	39.4 (±1.5)	36.0
Dissolved oxygen (mg/L)	3.86 (±1.07)	5.72 (±1.80)	3.11	4.70
Turbidity (NTU)	169 (±15)	96 (±12)	135 (±12)	5
Calcium (ppm)*	990 (±32)	503 (±15)	689 (±52)	386
Magnesium (ppm)*	2,873 (±84)	1,676 (±43)	2,033 (±108)	1,361
Sodium (ppm)*	25,133 (±275)	14,422 (±280)	16,692 (±807)	11,811
Potassium (ppm)*	926 (±27)	520 (±15)	629 (±28)	417
Strontium (ppm)*	22 (±1.5)	–	–	–
Chloride (ppm)†	–	24,075 (±624)	–	19,000
Sulfate (ppm)†	–	3,910 (±94)	–	2,700

Note: The average values of 6–20 measurements from different depths and locations each year are shown with their standard deviation. Concentration of calcium, magnesium, sodium, and potassium was analyzed using ICP-OES (*); the anions chloride and sulfate were analyzed using ion chromatography (†) only for the 2012 samples. Near-shore water measurements in brackish water zone are not included in the average 2013 values. Salinity was calculated by multiplying the conductivity value with 0.667 to obtain parts per thousand (ppt) value (Boyd, 2002).

parameters fluctuated between each sampling visit. For example, the average pH changed from 8.22 ± 0.05 to 8.58 ± 0.08 and back to 8.22 ± 0.2 in the 3 years of sampling. The corresponding conductivity readings in April 2011, June 2012, and June 2013 were 138 mS/cm (~92 ppt), 64 mS/cm (~43 ppt), and 59 mS/cm (~39 ppt), respectively, while ocean water collected from nearby Dim Bay in 2012 had a conductivity value of 53.9 mS/cm (~36 ppt). Water conductivity was measured during cursory visits to the island in May 2004, 2005, and 2009. The conductivity values during these 3 years were 98.3 mS/cm (~66 ppt), 108 mS/cm (~72 ppt), and 40.6 mS/cm (~26 ppt), respectively.

Calcium and magnesium hardness was measured in 2012 and 2013. The average calcium hardness in 2012 was 1328 ± 40 mg/L as $CaCO_3$ (532 ± 16 mg/L Ca), and that of magnesium was 6953 ± 296 mg/L as $MgCO_3$ (2005 ± 85 mg/L Mg). The respective Ca and Mg concentrations, as detected by ICP-OES, were 507 ± 16 and 1681 ± 49 ppm (mg/L). Alkalinity did not change much in the 3 years, with the highest value in 2011 of 178 ± 8 mg/L and lowest in 2013 of 140 ± 27 mg/L. Dissolved oxygen consistently showed a decreasing trend from the shallow to deeper water levels. For example, in 2011, the average dissolved oxygen decreased from 5.0 (± 0.6) mg/L in shallow waters to 4.1 (± 0.7) mg/L at ~25 cm, 3.3 (± 0.8) mg/L at ~50 cm, 3.4 (± 0.4) mg/L at ~75 cm, and 2.2 mg/L (± 0.1) at ~100 cm. Quantitative readings for dissolved oxygen could not be made in 2012 and 2013 due to error in instrument calibration. A vertical and lateral profile of the water characteristics is provided in the Supplementary Information along with comparison with previous investigations in the lake.

Saturation index values were calculated for carbonate minerals with the equilibrium-based PHREEQ software program and the measured chemical parameters of SL water. The calculated SI values indicate that the water conditions always remained supersaturated with respect to both aragonite and calcite (SI > 0.0). For aragonite, the SI values in 2011, 2012, and 2013 averaged 1.13, 0.94, and 0.95, respectively. The corresponding calcite SI values were 1.27, 1.08, and 1.09. The lower 2012 and 2013 SI values for both carbonate phases reflect the influence of a heavy rainfall event that occurred before and during water sampling visits to the lake.

Particulate material in SL water was examined by optical microscopy and found to be dominated by a variety of algae, bacteria, diatoms, and dinoflagellates, all of which contributed to the high turbidity (Supplementary Fig. S1). Comparisons made between settling rates of particulate material from SL with illite and smectite clay samples suspended in a 5% synthetic seawater solution are shown in Fig. 3. The turbidity values indicated that the lake water sample took ~180 days to reduce from a turbidity value of 121 to 8 NTU. In contrast, illite and smectite clays in the 5% seawater solution took only 11 and 6 h, respectively, to go from a starting turbidity of approximately 450 to 8 NTU.

3.2. Microbialite morphology and distribution

A representative transect of the distribution of microbialites identified in the northern section of SL is shown in Fig. 4. Several of the microbialite types have been previously described (Mann and Nelson, 1989; Neumann *et al.*, 1989) and include calcareous knobs (Fig. 5A), plateau-mushroom shaped (Fig. 5B), pinnacle mound (Fig. 5C), and cauliflower-top mushroom shaped (Fig. 5D) stromatolites. Although previously described, we observed that the near-shore calcareous knobs or bulbous crust (Neumann *et al.*,

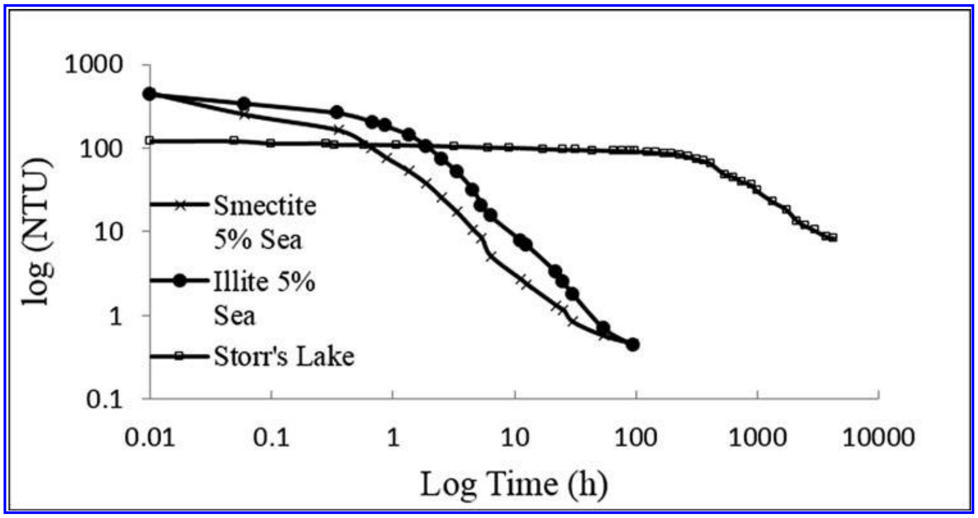

FIG. 3. Turbidity measurements in controlled environment, comparing SL particle settling rates with smectite and illite clays suspended into a 5% synthetic seawater solution. The relatively flat horizontal settling trends at the beginning of each test reflect the time taken for the suspended particles to move from the top of the water column in the vials to below the level of the light-scattering detector.

1989) exhibited two distinct features: (i) a lower, darker-colored, fused-granular, carbonate structure (~6 to 7 cm in thickness) by which the microbialite was attached to the lake bottom and (ii) an upper, lighter-colored carbonate structure (~5 cm thick) that had a smoother, continuous carbonate buildup compared to the granular bottom portion. A microbial mat with sporadic eukaryotic algal material was found between the grooves and on the uppermost surface.

It is important to note that both the cauliflower-top mushroom and the plateau-mushroom types described here possess the same overall external morphological appearance but varied in certain surface characteristics as described below (and also Supplementary Fig. S3). Additionally, the cauliflower-top mushroom reported here is the same as the ''mushroom type'' described by Neumann *et al.* (1989). The new terminologies, that is, plateau-mushroom and cauliflower-top mushroom types, were required to differentiate between the two morphologically different types of mushroom microbialites identified in our study. Both plateau-mushroom and cauliflower-top mushroom types were found at similar depths of 70–100 cm. The cauliflower-top mushroom microbialite had several bulging calcium carbonate knobs on the top surface, each resembling individual, smaller mounds, similar to the mushroom knobs reported by Neumann *et al.* (1989). These mounds began to disappear (~3 to 4 cm from the top) and were followed by continuous horizontal calcium carbonate laminations with intermittent branching or thrombolitic nodes. The laminations ended in the bottom stalk, which was very fragile and crumbled easily.

The uppermost surficial crust of the pinnacle mound microbialite was a continuous layer that was 0.5–1 cm thick on which the microbial mats were found in a scattered manner (Fig. 5C). A thrombolitic morphology involving a combination of branched and massive features that were ~7 to 8 cm thick was observed directly below the upper crust. These thrombolitic features were replaced below by a highly compacted region that extended between 5 and 6 cm. In its bottom-most region, the pinnacle mound exhibited stromatolitic layering for 1–2 cm. The single pinnacle mound that we collected was broken off as it was pulled from the soft muddy sediment at the base of the lake; thus the exact

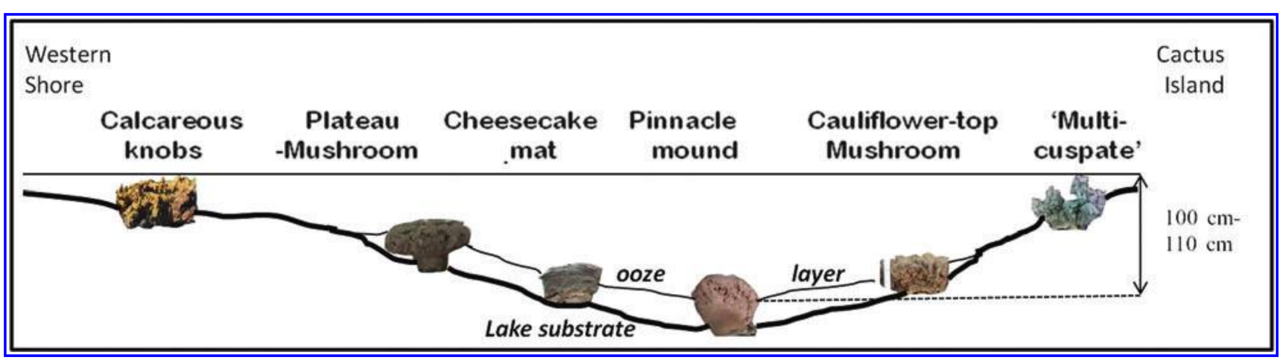

FIG. 4. Overview of the distribution of the microbialites in SL showing the approximate locations where the microbialites and water samples were collected in previous studies (Mann and Nelson, 1989; Neumann *et al.*, 1989) and current investigation. Horizontal distance from the western shore to Cactus Island is ~450 m.

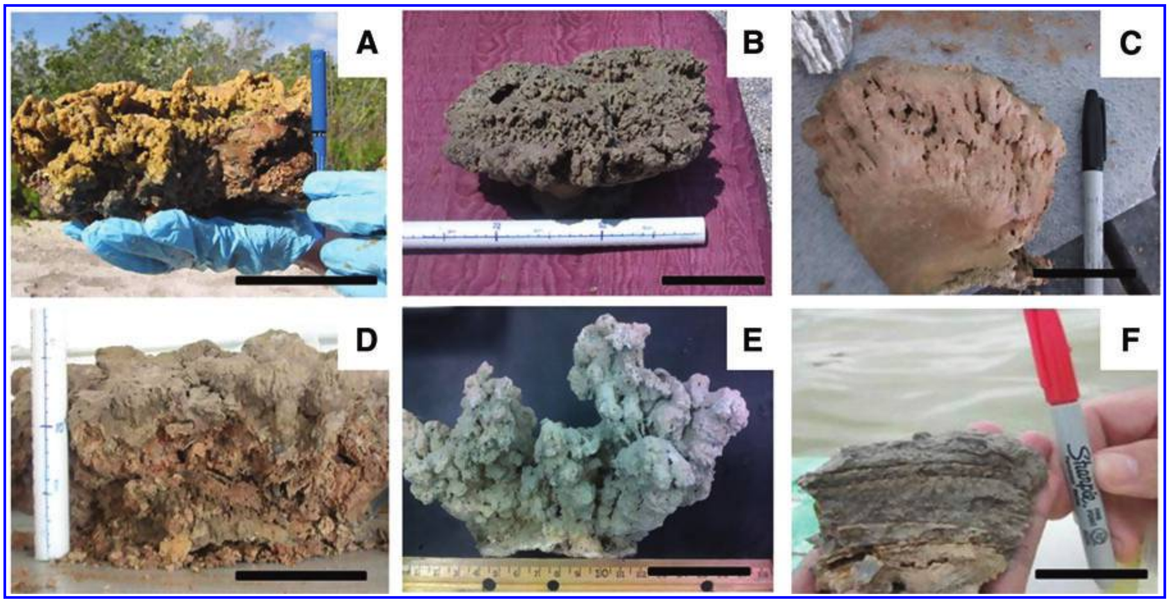

FIG. 5. Microbialites and microbial mats collected from SL. (**A**) Calcareous knobs; bar = 12 cm. (**B**) Plateau-mushroom; bar = 10 cm. (**C**) Half-sectioned pinnacle mound; bar = 7.5 cm. (**D**) Cauliflower-top mushroom; bar = 10 cm. (**E**) Multi-cuspate type; bar = 5 cm. (**F**) Cohesive but nonlithified cheesecake mat shown in cross-section profile; bar = 7.5 cm.

length of this type of microbialite could have been longer than that described here (*i.e.*, ∼17 cm). The frequency of lithified microbialite structures decreased in the deepest portions of the lake, except for the occasional, broken calcified knobs that were submerged in ∼30 cm thick gelatinous bottom material (termed as ooze).

Moving toward Cactus Island, another microbialite morphotype was identified at a depth of about 46–50 cm, here referred to as the ''multi-cuspate.'' The distribution of the multi-cuspate microbialites was fairly continuous from the point it began to appear but was less frequent in the shallow water toward the shore of Cactus Island. The multi-cuspate microbialites were morphologically different from the other morphotypes owing to their more distinguished protrusions and sharper edges (Fig. 5E). The closest resemblance was to the calcareous knobs that were located at similar depths but on the other end of the transect along the western shore of SL. The multi-cuspate structures were well lithified and did not crumble easily (Supplementary Fig. S4). The bottom 1 or 2 cm of the multi-cuspate microbialite was layered and seemed to represent the locations by which it was anchored to the lake bottom sediment. Similar bottom layering was also found in the pinnacle mound microbialite. On top of this layered profile, the microbialite began to form a massive carbonate structure, which eventually proliferated to result in sharper edges of varying lengths, resembling several fused cusplike formations. These large (∼3 to 5 cm) protrusions distinguished these microbialites from the calcareous knobs. The multi-cuspate microbialites possessed limited microbial mat material on the top surface unlike the other microbialite types found in SL, with occasional gelatinous green and pink material found scattered on the grooves and flatter surfaces.

A well-laminated, cohesive, but weakly lithified and flat-lying ''cheesecake'' microbial mat was found to be present on top of the gelatinous material (ooze) in most lake-bottom locations (Fig. 5F). This mat type was particularly abundant in the region between the plateau-mushroom and pinnacle mounds, and the multi-cuspate microbialite and Cactus Island shore. The laminations in the cheesecake mat extend to about 7–8 cm depth from the top of the sediment layer. A loose and friable, calcified layer existed below the laminations. The laminations disappeared below this calcified layer and were replaced by the soft yet cohesive gelatinous material that extends below for approximately 30 cm, till it reaches the hard, bottom layer of the lake. The cheesecake mat was the only microbial mat collected that was not associated with the lithified microbialite heads.

3.3. Light penetration in Storr's Lake water

Due to the high turbidity of the SL water, it was essential to determine the amount of light available for the phototrophs in the microbial mats located at different depths in the water. The Secchi disk method was used to determine light penetration at two similar locations, where the calcareous knob microbialites were identified (June 2012). The white portion of disks was not visible below depths of 17–26 cm, and the black portion disappeared below depths of 15–20 cm. Neumann *et al.* (1989) reported depths of 46 cm below which the Secchi disk disappeared during their December 1987 study.

Light intensity was also measured by HOBO pendant loggers with results shown in Fig. 6. In 2012, the probe was initially set into the location adjacent to the top of calcareous knob microbialites at a depth of 40 cm. The Day 1 readings were collected on an overcast and mostly cloudy day and recorded a maximum signal of ∼1150 to 1200 lumens/ft^2 (107–112 lumens/m^2). The probe was removed from the water and exposed to direct sunlight above the water surface during Day 2, where a maximum reading of ∼20,000 lumens/ft^2 (1,860 lumens/m^2) was obtained. The

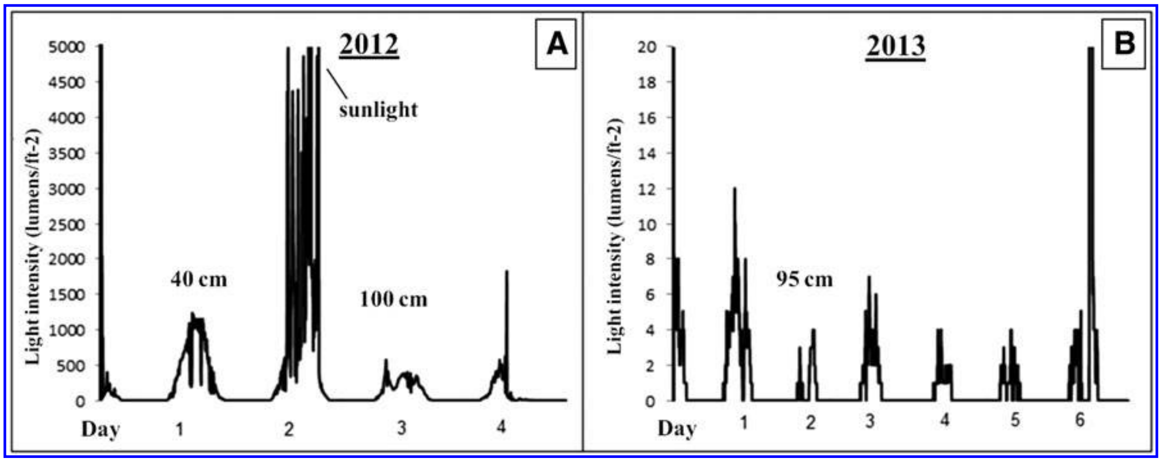

FIG. 6. Light-intensity data collected using HOBO logger anchored into the bottom sediment and set at a depth equivalent to that of the microbialite heads. The graph shows the data from day and night cycles recorded in (**A**) 2012: Day 1, probe placed next to calcareous knobs (at 40 cm depth); Day 2, probe exposed to direct sunlight above the water (the *y* axis in the plot is cut off at 5000 lumens/ft^2, but the actual value when exposed to sunlight reached $\sim$20,000 lumens/ft^2); Day 3, probe left at 100 cm depth; Day 4, probe removed from lake water—the small spike at $\sim$1800 lumens/ft^2 was due to exposure to surface sunlight under overcast conditions. (**B**) 2013: Probe emplacement at a depth of $\sim$95 cm for the entire 6 days. The spiked value at the end of the run at Day 6 was produced when the probe was exposed to sunlight under overcast conditions. The *y* axis in the plot is cut off at 20 lumens/ft^2, but the total subaerial light intensity on Day 6 was $\sim$5100 lumens/ft^2.

same day, the probe was then moved and inserted at the same height as the top of a plateau-mushroom microbialite at a depth of about 100 cm and kept in this position for 2 days. The weather patterns changed from partly cloudy on Days 2 and 3 to scattered rain on Day 4. The light intensity during Days 3 and 4 at the plateau position varied from 200 to 600 lumens/ft^2, or between 1% and 3% of the surface light intensity.

In 2013, the probe was placed at $\sim$95 cm next to the top of the plateau-mushroom shaped microbialite and left in place for 6 days. The highest intensity of light at this depth was recorded at 12 lumens/ft^2 (1.12 lumens/m^2) relative to the surface, where a maximum intensity of $\sim$5100 lumens/ft^2 was obtained. This represents a decrease in luminosity with 96 cm of water depth of approximately 99.8%. The lower light intensity values in 2013 as opposed to 2012 were due to the heavy overcast conditions. Unfortunately, the overcast and rainy conditions present during both our 2012 and 2013 sampling intervals prevented us from making any recordings under full sunlight conditions with the HOBO pendants.

3.4. Mineralogy and microscopic characterization of the microbialites

Magnesium calcite was the dominant mineral found in homogenized composite samples of all five microbialite types prepared and analyzed separately by XRD. Aragonite was detected only in the pinnacle mound, plateau-mushroom, and in smaller quantities ($\sim$3%) in the multi-cuspate type.

A second set of XRD analyses was conducted, with individual samples being collected from multiple positions within the plateau-mushroom and pinnacle mound microbialites to discern whether they displayed any spatial variability with respect to both aragonite and Mg-calcite contents (Fig. 7). The pinnacle mound (PM) microbialite contained aragonite in the top 1 cm surface section (PM-1b-C); however, no aragonite was detected in the sample collected at a 2 cm depth below the top surface (PM-2b-C) and in the central core of the sample located 9 cm below the surface. Aragonite percentages were highest at the base of this microbialite (PM-3b-S to PM-4b-C) and at the lateral surfaces (PM-6-S). In the plateau-type microbialites, both lateral surficial (Plateau-S) and core (Plateau-C) samples had some of the highest proportions of aragonite detected in SL microbialites, though the aragonite/calcite ratios decreased outward; 76/24 for core versus 48/52 for surficial sample, respectively. Although the aragonite/calcite ratios varied from site to site within the microbialites, no particular trend was observed with regard to water depth or distance from the shore in the microbialites that were evaluated.

Insoluble components were not detected as residues by visual inspection following deionized water rinse (to remove salts) and a 5% nitric acid digestion step performed on 11 sections of the microbialite heads. Calcite with variable mol % Mg (7.5–15.6%) was identified as the dominant mineral type in all samples analyzed by combined ICP-OES (Table 2) and XRD analyses (Fig. 7). Concentrations of Si and Na were at, or just above, detection limit (*i.e.*, 10 ppm), while Fe, K, Mn, and Al concentrations were all below detection. An explanation for the correlation between the elemental concentration and XRD mineralogy is provided in Supplementary Fig. S5.

Preliminary investigation with reflected light microscopy of thick, epoxy-coated sections of the pinnacle mound microbialites revealed grains that were generally subrounded, sand-sized, and present in a layered format (Supplementary Fig. S6). Many of the rounded grains appeared to be zoned, often with one overgrowth layer, rarely two, around a central core grain. Most grains were in contact with each other in the 2-D X-sections. However, in a couple of locations, these grains were isolated and not in proximity with the

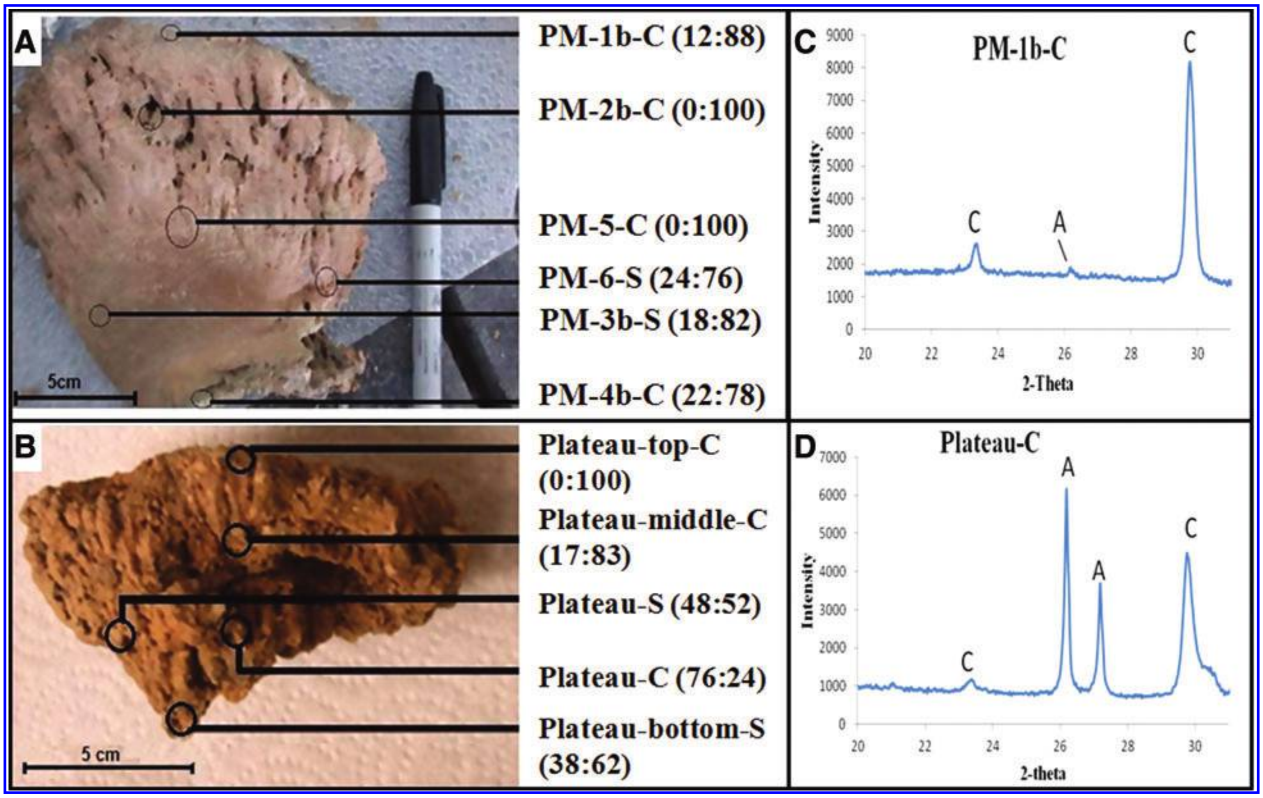

FIG. 7. Microbialite samples depicting the various positions where samples were collected for XRD analysis. (**A**) Half-sectioned pinnacle mound (PM) and **(B)** half-sectioned plateau-mushroom shaped microbialites. Samples were collected either in the center, C, or at surface, S. Numbers to the right of the sample locations in (A) and (B) correspond to the aragonite:calcite percent ratio as determined by XRD analysis. Examples of XRD pattern for two of the samples, PM-1b-C (**C**) and Plateau-C (**D**), show peaks for aragonite and calcite, shown by the letters A and C, respectively.

neighboring grains. A couple of grains of *Homotrema rubrum* could be seen. Porosity, as seen by epoxy-filled cavities, was also observed.

Microscopic investigation of the microbial mat in the plateau-mushroom microbialite indicated that, in addition to the microorganisms, there were abundant gelatinous features (EPS) with various dark, amorphous grains (data not shown). These irregular grains reacted with 1 *N* HCl and produced CO_2 bubbles, indicating that those were carbonate minerals. Some of the EPS material also exhibited effervescence with

TABLE 2. ICP-OES RESULTS FOR THE ACID-DIGESTED MICROBIALITE SOLID SAMPLES SHOWING THE PROFILE POSITIONS AS NOTED IN FIGURE 7, THE Σ m*M* VALUES OF Ca, Mg, AND Sr RECOVERED FROM THE DIGESTION OF 0.25 g OF SOLID IN 10 mL OF SOLVENT

Sample	*m*M		*Molar Ca:Mg ratio*	*Molar Mg:Ca ratio*	*Mol % Mg*	*Total Sr* (*m*M)
	Ca	*Mg*				
Pinnacle mound						
PM-1b-C	201	35.2	5.7	0.18	14.9	0.06
PM-2b-C	212	33.0	6.4	0.16	13.6	0.11
PM-3b-S	207	16.7	12.4	0.08	7.5	0.26
PM-4b-C	195	34.7	5.6	0.18	15.6	0.13
PM-5-C	211	36.2	5.8	0.17	14.6	0.07
PM-6-S	216	34.6	6.3	0.16	13.7	0.07
Plateau						
Plateau-top-C	203	32.9	6.2	0.16	14.2	0.09
Plateau-middle-C	219	34.5	6.3	0.16	13.7	0.10
Plateau-bottom-S	217	32.4	6.7	0.15	12.7	0.18
Plateau-C	215	18.3	11.7	0.09	7.9	0.29
Plateau-S	227	21.0	10.8	0.09	8.4	0.22
Vein calcite	259	0.09	2742	Insignificant	Insignificant	Not analyzed

The molar ratio of Ca:Mg and the molar Mg percentage in the samples is also shown.

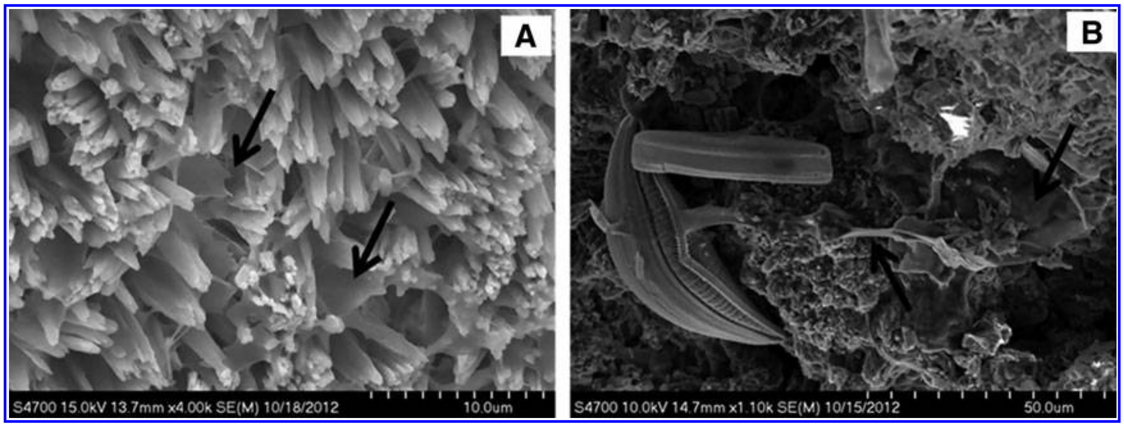

FIG. 8. Scanning electron microscope images of the microbialite structures. (**A**) Acicular crystals, characteristic of aragonite, found in the lower section of plateau-mushroom microbialite. (**B**) Diatoms in the microbialites of SL. Remains of EPS material are indicated by black arrows.

HCl, revealing that these polymeric substances might also have carbonate material present in them. Similarly, examination of the water column showed rare, dark, carbonate particles in the midst of dispersed microbial and EPS assemblage.

Scanning electron microscopy–energy dispersive spectroscopy analysis of the microbialites showed a variety of internal and external morphological features (Fig. 8). The microbialites were dominated by calcium carbonate crystals, with 0.5–3.9 atom % Mg. The morphology of the crystals ranged from irregular to angular, blocky, needle- and triangular-shaped, with calcium carbonate–encrusted cyanobacterial filaments and remains of EPS. The plateau-mushroom and pinnacle mound microbialite exhibited occasional needle-shaped structures, suggesting an aragonitic mineralogy (Fig. 8A). Remains of diatoms, such as *Navicula*, were also observed to be present (Fig. 8B).

3.5. Microbial mat diversity

Cultivation-independent microbial diversity analyses were performed on the five different types of microbial mats (*i.e.*, calcareous knob, plateau-mushroom, pinnacle mound, cauliflower-top mushroom shaped, and cheesecake) isolated from SL. Amplicon libraries of the partial 16S rRNA genes (V1–V3 region) were sequenced and clustered into operational taxonomic units (OTUs) at 97% similarity or greater. The summary of the data obtained from the pyrosequencing method is shown in Table 3. A total of 126,576 barcoded sequences was recovered after sequence trimming and filtering by using mixed and dots filters. The mixed filter removed reads that occurred as a result of simultaneously sequencing a mixture of different DNA molecules, whereas the dots filter removed sequences with three successive nucleotide flows that recorded no incorporation. The average read length of the sequences was 471 bp. The five different mat types had between 15,782 and 31,862 sequence reads and were clustered into OTUs with QIIME software (Caporaso *et al.*, 2010).

Alpha diversity index values (Table 3) were calculated based on equalized sequences and indicate that all five microbial mat types exhibited high diversity. Chao 1 values, which were used to estimate species richness, indicate that the deeper-water plateau-mushroom microbial mat had the largest estimated diversity (20,915), whereas the lowest was for the shallow-water calcareous knobs (7,743). The mat on the plateau-mushroom also had the highest Shannon index values (12.03). The Chao1 values correspond well with the Shannon index and observed species values. The distribution of species was most even in the plateau type and closely followed by the other microbial mats as shown by the equitability values.

Among the OTUs identified, only 24% of the recovered sequences were shared between all five microbial mats, suggesting that each mat type had a distinctive community. The relatedness between the five microbial mat communities was also calculated with beta diversity analysis. A distance tree was constructed by using the unweighted pair group method with arithmetic mean (UPGMA). Jackknife analysis allowed repeated subsampling of a subset of data from each sample, providing a final robust distance tree (Fig. 9A). The mat on the shallow-water calcareous knob was most similar to the plateau-mushroom microbial mat in terms of microbial population. These two mats clustered closest with the cheesecake microbial mat that was found on top of the gelatinous material covering the lake bottom at deeper-water locations. The deep-water pinnacle mound microbialite grouped closely with the cauliflower-top mushroom microbialite. Both of these latter two types of microbialites are located farther away from the western shore of the lake and are submerged to greater water depths.

The bacterial composition of the five mats fell into 12 major bacterial phyla, each distributed in various relative percentages among the mats (Fig. 9B). Though a large amount of sequences was recovered, the analysis of only a partial length (V1–V3) of the entire 16S rRNA gene allowed identification only up to the family level of taxonomy, with few sequences reaching only to level of class or order. The cheesecake microbial mat had approximately one-third (36%) of its OTUs as unclassified, which was the highest among the five mat types. The shallow-water calcareous knob had the lowest percentage (12%) of unclassified bacteria present. Chloroflexi constituted approximately half ($\sim$46%) of the entire bacterial population identified in both the deeper-water cauliflower-top mushroom and pinnacle

TABLE 3. SUMMARY OF THE BACTERIAL 16S rRNA GENE DIVERSITY ANALYSIS BY THE PYROSEQUENCING METHOD

	Calcareous knobs	*Plateau*	*Cheesecake*	*Mushroom*	*Pinnacle mound*
Sequences	31,862	30,608	28,082	20,242	15,782
OTUs[a]	5,636	12,261	9,096	6,859	4,897
Singletons[a]	3,083	8,118	5,872	4,493	3,075
Doubletons[a]	852	1,774	1,355	1,020	795
Equalized sequences[b]	14,500	14,500	14,500	14,500	14,500
Chao1[c]	7,743 (±236)	20,915 (±725)	15,697 (±347)	14,218 (±262)	10,507 (±183)
Chao1 confidence[d]	7,343/8,054	20,217/22,302	15,209/16,213	13,873/14,547	10,260/10,800
Shannon[c]	10.07 (±0.02)	12.03 (±0.02)	11.25 (±0.02)	10.90 (±0.01)	10.49 (±0.01)
Observed species[c]	3,595 (±37)	7,340 (±41)	5,840 (±42)	5,501 (±23)	4,646 (±14)
Equitability	0.82	0.92	0.88	0.87	0.86
% Coverage[e]	90.3	73.4	79.1	77.8	80.5

[a]Values calculated based on 97% similarity threshold.
[b]Number of equalized sequences used to generate the diversity indices, such as Chao1, Shannon, observed species.
[c]Average values ± standard deviation of diversity using 10 iterations of randomized sequences.
[d]Chao1 lower and upper confidence limits at 95%.
[e]Based on Good's coverage estimator.

mound mats, while calcareous knob, plateau-mushroom, and cheesecake types had only 16–20% Chloroflexi. Within the phylum Chloroflexi, anaerobic halorespirers, Dehalococcoidaceae made up to 24% in the cauliflower-top mushroom and 21% in the pinnacle mound. Other members included several bacteria under the class Anaerolineae and order Dehalococcoidetes (family Dehalococcoidaceae falls under this order). Members of the yet-uncultured OPB11 order, which is thought to include several green nonsulfur bacteria (Hugenholtz *et al.*, 1998), were present in notable

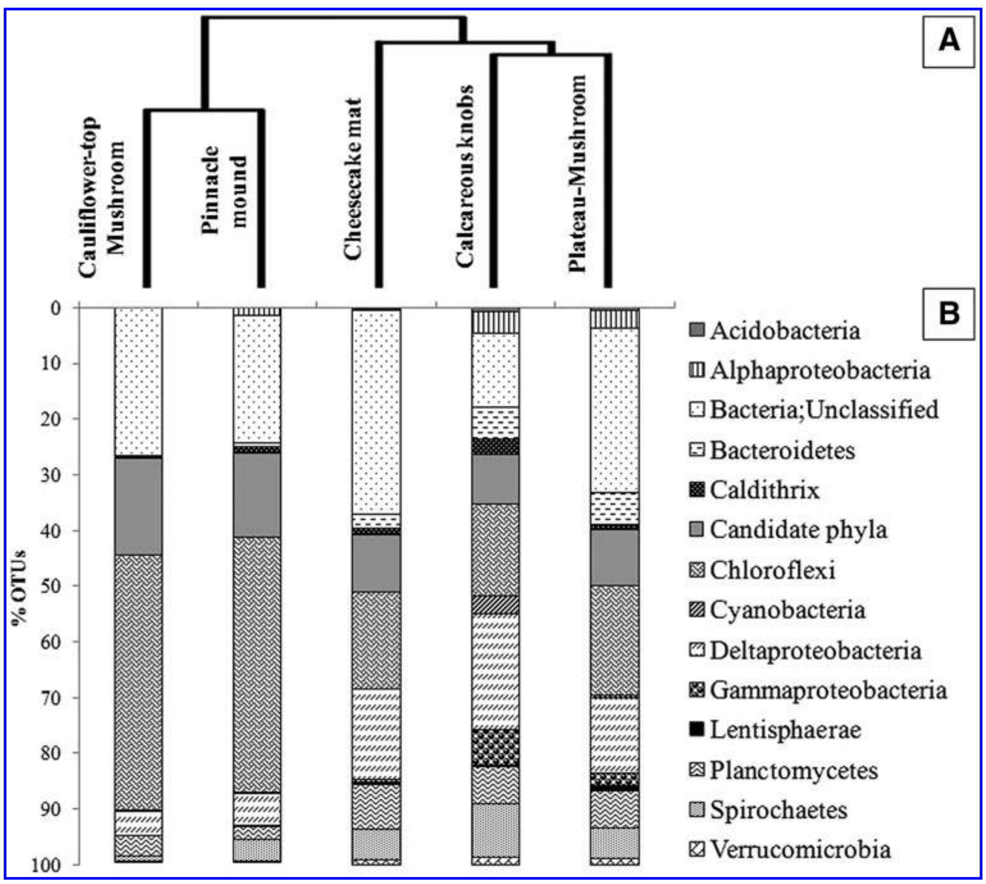

FIG. 9. (**A**) Dendrogram showing the relationship between the different microbial mats in SL acquired by jackknifed UPGMA clustering method. The scale bar indicates the evolutionary distance between the communities and has a value of 0.05, meaning 0.05 nucleotide substitutions per sequence position. (**B**) Relative percentage abundance of major bacterial taxa detected in five SL microbial mats by analysis of the 16S rRNA gene. Twelve different major taxa are reported along with significant percentages of candidate phyla and unclassified bacteria. Note: Plateau indicates plateau-mushroom microbialite, and mushroom indicates cauliflower-top mushroom microbialite.

quantity, especially in the pinnacle mound and cheesecake mat (~9% in each). The class Deltaproteobacteria includes several SRB that were enriched in the shallow-water calcareous knob (21%), followed by the cheesecake mat (16%). The lowest percentage of Deltaproteobacteria occurred in the deeper-water pinnacle mound (5%) and cauliflower-top mushroom (6%) mat types. The SRB family, Desulfobacteraceae, dominated the recovered Deltaproteobacteria sequences. For example, 16% of the 21% of Deltaproteobacteria were represented by Desulfobacteraceae. Other significant SRB members in this class included family Desulfohalobiaceae and Desulfovibrionaceae. The other taxa represented in all mat types included the Spirochaetes, Planctomycetes, Alphaproteobacteria, Gammaproteobacteria, Bacteroidetes, and Caldithrix. Purple nonsulfur bacteria of families Rhodospirillaceae and Rhodobacteraceae belonging to the class Alphaproteobacteria were detected only in the plateau-mushroom and calcareous knob microbialites.

Several members of the phyla discussed above include halophilic and brackish-living bacteria, with many of them also being photosynthetic (*e.g.*, order Chromatiales and family Chromatiaceae in the Gammaproteobacteria) and able to survive in anoxygenic environments (Imhoff, 2006). Vibrionaceae is yet another anaerobic, phototrophic Gammaproteobacteria that represented ~4% of the total calcareous knob population. Cyanobacteria were detected at low levels in all the mat types ranging between <1.0% and 3.0%. The highest levels of cyanobacteria were observed in the shallow-water calcareous knobs (~3.0%) and included families Cyanobacteriaceae, Pseudanabaenaceae, and Phormidiaceae, and order Chroococcales. The other mat types had less than 1.0% relative abundance of cyanobacteria. Other taxa, such as Acidobacteria, Verrucomicrobia, and Lentisphareae were below 1.0%, while Firmicutes, Actinobacteria, Chlorobi, Elusimicrobia, Betaproteobacteria, and Epsilonproteobacteria were present at less than 0.1% (Supplementary Table S2). A relatively high proportion of the mat population was classified as candidate phyla, which include bacteria that have not yet been cultured in the laboratory but whose existence has been observed through 16S rRNA gene analysis. For example, 11% and 8.0% of the cauliflower-top mushroom and pinnacle mound population, respectively, were represented by the order HMMVPog-54. These have previously been identified in methane-rich biofilm communities with a high diversity of Deltaproteobacteria (Lösekann *et al.*, 2007). Additionally, bacteria from the phyla WS3 (Dojka *et al.*, 1998) occupied anywhere from ~0.6% in cauliflower-top mushroom shaped to a maximum of ~3.4% in calcareous knobs.

4. Discussion

4.1. Physical, chemical, and optical characterization of Storr's Lake water

Water parameters, such as depth, salinity, local turbidity, and so on, in SL exhibited high fluctuations that are primarily influenced by rainfall events (Table 1). The main body of water was always turbid during field analysis, but a relatively clear-water brackish lens zone developed adjacent to the shoreline following periods of rainfall. The associated brackish-saline mixing zone migrated outward into the deeper portions of the lake during periods of high meteoric water runoff (Fig. 2B). Previous studies have reported that rainfall events can cause considerable dilution of the lake water and result in lowered salinity and an increase in the metabolism of the phototrophic community in the lake (Pinckney *et al.*, 1995; Paerl *et al.*, 2003). The lowering of salinity following rain events was confirmed in the present study, and we believe that our May 2009 recording of ~26 ppt is the lowest salinity reading ever recorded for SL. This lower-salinity period can enable opportunistic gastropods and fish species to occasionally colonize the lake (Garrett, 1970; Supplementary Fig. S2).

The reddish-brown color in the lake is imparted by two sources: (i) the organic tannins brought in by the brackish water draining into the lake that were derived from decaying plant material and (ii) the presence of planktonic communities of halophilic algae and bacteria, which are usually enriched in carotenoid pigments that contribute to the reddish coloration (Mann and Nelson, 1989; Oren and Rodríguez-Valera, 2001). Bacteria, algae, and most organic material have a net negative surface charge, causing these particles to repel from each other, enabling the material to become colloidal and remain suspended rather than settling to the lake bottom. The long-term suspension of particles in the water (Fig. 3) supports the colloidal nature of the particles. Motile planktonic microorganisms seeking sunlight for their metabolism would also move toward the surface of the water during day. Neumann *et al.* (1989) suggested that oxygen gas released from the gelatinous thrombolitic mounds also carried some of the mat material to the surface. A similar process, possibly involving other gas components as well, could be presumed to occur with the microbial mats at deeper depths. Additionally, high wind activity seen in the lake could possibly agitate the water and thus keep the particles suspended, although the stratification observed in dissolved oxygen profiles suggests that complete and rapid vertical mixing is hindered. It should be noted that tidal flow has only a minimal effect on the lake due to limited connectivity to the ocean, though abnormal high or low tides could influence the lake parameters (Mann and Nelson, 1989). Density changes due to seasonal or diurnal warming-cooling and evaporative concentration of dissolved components also could conceivably play a role in water mixing. In addition to the above factors, freshwater inflow during rain and storm events would also affect the changes seen in turbidity, pH, salinity, and other water parameters.

The average turbidity was 96 (± 12) and 135 (± 12) NTU, during 2012 and 2013, respectively. Likewise, the light intensity reaching depths of ~100 cm in both these years was 200–600 and 12 lumens/ft^2, respectively, ranging from 0.2% to 3.0% of the intensity of sunlight reaching the surface of the lake. The limited sunlight reaching the bottom was scattered between particles as it penetrated through the water column (Figs. 3 and 6). It is thus interesting that some photosynthetic communities survive even in the deeper microbialites that are located in the dim-light conditions (Fig. 9B). In one recent study, cyanobacterial mats showed maximum photosynthetic efficiency under limited light conditions (Al-Najjar *et al.*, 2012). The wavelengths of the penetrating light are also important in governing the phototrophic system. For a cyanobacterial photosynthetic community to function, it requires light of wavelengths between 400 and 700 nm (Jørgensen *et al.*, 1987). However, some photosynthetic communities are capable of surviving in wavelengths of the extended spectrum (UV and IR), having developed specialized pigments and enzymes capable of using wavelength fractions (Castenholz and García-Pichel, 2000; Kühl *et al.*, 2005). Phototrophic green sulfur bacteria, for example, contain light-harvesting chlorosomes that make them well-adapted to survive in low-light conditions (Frigaard and Bryant, 2004). The light probe used for SL water analysis measured a full array of wavelengths from 200 to 1100 nm but unfortunately does not differentiate between the different wavelengths. However, in the case of SL, the shorter-wavelength UV spectrum would be expected to be more penetrating and, thus, extend to deeper sections of the lake. Also, the small amount of light reaching to depths of $\sim$1.0 m appears to be able to support a photosynthetic community on the microbialites based upon our microbial diversity results (Fig. 9B). Future investigations into the spectrum of light used by the microbial communities in SL would be of great interest.

4.2. Distribution and mineralogy of microbialites

The external morphology of the cauliflower-top mushroom microbialite identified in our study was similar to the previously reported plateau-mushroom type (Mann and Nelson, 1989; Neumann *et al.*, 1989), but closer observation revealed differences in laminations and appearances (Supplementary Fig. S3). Hence, the cauliflower-top mushroom and plateau-mushroom were separately categorized in this study. In addition to the previously identified microbialites, we described a new morphotype of the microbialite termed ''multi-cuspate'' that had limited microbial mat material. The lack of prominent microbial mat development on the surface of the multi-cuspate microbialites was not a reflection of water depth, since these were located at almost the same water level as the calcareous knobs. Since microbial mat coverage and thereby the activity of mat organisms are inferred to be inadequate, the multi-cuspate type could be categorized as a ''sub-fossil.'' The exact reason for the limited microbial mat cover on the multi-cuspate microbialite is still unknown and is worthy of further investigation.

Similar to other environments that harbor microbialites, the overall microbialite morphology is generally accepted to be primarily controlled by environmental factors, though the microorganisms play the role of actual accretion and fabric development (Dupraz *et al.*, 2006). One of the major controls is the water depth of SL, and in turn the availability of light for the microorganisms, especially phototrophs. The flat top of the slightly deeper plateau microbialite has also been interpreted as the lowest water level in the lake (Mann and Nelson, 1989). The bulging nature toward the top of the microbialites indicates that the area closest to the surface is the most productive region, where maximum light is accessible and water depth is conducive.

A considerable amount of aragonite was identified in the pinnacle mound and plateau-mushroom microbialites (Fig. 7). All previous studies of SL microbialites have reported only the presence of Mg-calcite and no aragonite (Hattin, 1983; Pentecost, 1989; Neumann *et al.*, 1989; Fowler, 2011; Dupraz *et al.*, 2013). We observed that the mol % Mg in the carbonate minerals of the pinnacle mound–type microbialites initially decreased from the top to middle positions (PM-1b-C to PM-3b-S) but then increased, moving from the middle toward the bottom of the microbialite (PM-4b-C). The aragonite percentage decreased from PM-1b-C to PM-2b-C and PM-5-C and then increased again, reaching the highest values with samples PM-4b-C and PM-6-S (22% and 24% aragonite, respectively; Fig. 7A and 7B; Table 2). It should be noted that the bottom, calcified, ground substrate of the lake, on which the microbialites develop, is aragonitic in composition. However, the microbialite samples chosen for XRD analysis were carefully sectioned only from the microbialite structures themselves (exact locations as shown in Fig. 7), thereby rendering any influence of the hard lake substrate negligible.

The presence of aragonite was further confirmed by the correlation seen between Sr and Mg concentration (Table 2, and Supplementary Fig. S5). The large radius of Sr^{2+} (1.18 Å) is more readily accepted into the aragonite structure, while the smaller Mg^{2+} ion (0.72 Å) gets preferentially incorporated as a replacement for Ca^{2+} (1.00 Å) in calcite (Krauskopf and Bird, 1994). Calcite can accept a higher proportion of Mg in its crystal structure relative to aragonite, especially when the calcite is precipitated in biologically mediated reactions (Weiner and Dove, 2003). Aragonite does not readily accept Mg in its crystal structure; thus the aragonite content should be inversely correlated with Mg concentration. The results obtained generally support this expectation, but there were clear anomalies. For example, both the aragonite percentage and Mg content reach their maximum values with sample PM-4b-C (22% aragonite and 15.1 mol % Mg; Table 2). Therefore, the Mg/Ca ratios may be controlled by processes associated with calcite formation rather than exclusionary processes arising from the formation of aragonite.

Two sources are likely attributed to the origin of aragonite in the microbialites: an *in situ* biogeochemical precipitation and/or detrital grains that are blown over from the nearby East Beach and incorporated into the structure. The saturation state of the carbonate minerals in water has been shown to be an essential component in determining microbialite development (Dupraz and Visscher, 2005). The SI values for current SL water samples as determined with the PHREEQ program indicate that calcite precipitation is favored over aragonite, based on equilibrium modeling. Though the microbial mats can drastically alter the availability of ions, such as calcium and bicarbonate in the microenvironment that they create (Dupraz *et al.*, 2009), the characteristics of the water above them are also important in controlling the mineralogy of the microbialites. The calcite and aragonitic composition in SL microbialites could thus be partially or completely dependent on the past composition of the lake water. Storr's Lake began to form around 3100 years ago due to shifting tidal sands that closed inlets (Zabielski, 1991). Carbon dating revealed that the microbialites began to form at least 2310 years ago (Paull *et al.*, 1992). Terrestrial and evaporative processes likely would have increasingly influenced the lake water composition after the basin became isolated from direct tidal input. Given the fluctuations observed in the lake water parameters, including ''freshening events'' and periods of hypersalinity noted in previous studies (Pinckney *et al.*, 1995; Paerl *et al.*, 2003; Park, 2012) and this investigation, it is likely that the lake has experienced similar and possibly even more drastic changes in its composition during its 3100-year history.

Figure 8A shows the characteristic acicular morphology of aragonite. The close association of these grains with calcified EPS reveals that the aragonite crystals are likely autochthonous. Previous thin-section studies on SL and other inland, hypersaline lake systems (*e.g.*, Salt Pan, Eleuthera Island) show micritic fabric in the form of peloids, micropeloids, spheres, and subcircular morphologies within the microbialite (Neumann *et al.*, 1989; Paull *et al.*, 1992; Dupraz *et al.*, 2004; Glunk *et al.*, 2011). These morphologies have almost exclusively been associated with *in situ* precipitation by entombment of bacteria, precipitates initiated at the EPS matrix, multiphase dissolution, re-precipitation, and so on.

The incorporation of the other calcium carbonate–forming organisms, such as gastropods (Neumann *et al.*, 1989), ostracodes (Park, 2012), foraminifera, and diatoms in the microbialite structure, could also influence the variation seen in mineralogical composition. Beach sand materials that occasionally wash in during hurricanes along the eastern shore of SL adjacent to low-lying coastal dunes along East Beach (located northeast of SL) and Dim Bay have been reported (Park, 2012). As seen in our preliminary reflected microscopic analysis, the grains exhibit a wide range of morphologies, with the majority showing rounded to subrounded grains that are closely packed and cemented, while individual grains also appear to be present with little or no contact (Supplementary Fig. S6). Previous thin-section studies on the microbialite structures in enclosed SL did not report detrital grains (Neumann *et al.*, 1989; Paull *et al.*, 1992) or that the entire microbialite head was precipitated *in situ* through chemical and/or biological processes. Our observation contrasts with those of previous researchers in that we observed grains that appeared to be detrital. Wind-blown detritus may conceivably be carried across the entire lake during intense storm activity, along with possible foraminifera, and incorporated into the microbialite structure. Intertidal sands collected from East Beach were noted to be enriched in foraminifera, such as *Homotrema rubrum*. It is also important to note that *H. rubrum* and other forams are made up of high Mg-calcite and thus are not a likely source for aragonite in the microbialites. Whether the heavier aragonitic beach sands were blown into the lake is questionable, but such a process may occur during episodes of strong winds associated with storm activities. Therefore, the presence of detrital grains in the microbialite structure is evidenced, but a more extensive thin-section microscopy study is needed. Diagenesis and recrystallization may also influence the mineralogy of the microbialites. The observed zoning of a Mg-calcite-rich core zone surrounded by more aragonite-enriched exterior zones (Fig. 7; Table 2) may reflect diagenetic transformation of aragonite to calcite over time, especially if the cores of the pinnacle mound types represent older microbialite growth.

4.3. Microbial mat diversity

Earlier studies of SL microbialites have described the physical nature of the microbial mat and microbialites (Mann and Nelson, 1989; Neumann *et al.*, 1989; Paerl *et al.*, 2003; Dupraz *et al.*, 2006). However, few molecular studies have been performed to investigate the microbial diversity of the mats, and those prior examinations were focused specifically on the near-shore and shallow-water calcareous knobs (Brigmon *et al.*, 2006). The present study provides a more comprehensive coverage of the microbial population in mats on the surface of four different microbialites and the cheesecake mat that is associated with the lake bottom sediments (Table 3). Although funding limitations prevented an analysis of duplicate morphological samples to examine the horizontal variation within a mat type, we were able to generate a more comprehensive survey of the microbes present within the different mat types (Table 3). Clustering analysis revealed that the cauliflower-top mushroom and pinnacle mound clustered together in the UPGMA tree, indicating that the bacterial diversity and abundances were phylogenetically comparable between these two types (Fig. 9A), whereas the calcareous knob and plateau-mushroom type grouped together. The cheesecake mat was collected from a location (labeled as "ooze" in Fig. 4) between the calcareous knob–plateau and the offshore cauliflower top–pinnacle mound pair, thus potentially representing a transition microbial population between the two groups. A high percentage of the bacterial population (11–36%) in all mat types was unknown, suggesting that potentially novel and previously unidentified microorganisms are present in the SL mats (Fig. 9B).

The amount of cyanobacteria detected was extremely low (*e.g.*, 0.01% in the pinnacle mound). It is important to note that cyanobacteria are typically larger than other bacteria and hence occupy more volume. Thus, the total percentage of cyanobacteria reported through microbial diversity analysis does not correlate with the volume that is present in the microbial mats. The high turbidity of the lake water and consequently the lower amount of sunlight (Fig. 6) reaching the deeper portions are the most likely explanation for this lack of abundant light-dependent cyanobacteria on the SL pinnacle mounds. Hypersaline conditions could also contribute to the reduced presence of cyanobacteria (Paerl *et al.*, 2003; Marcarelli *et al.*, 2006). Though these phototrophic microorganisms are capable of growing in hypersaline conditions and generally have a wide range of salt tolerance (Green *et al.*, 2008), the activity and population can be negatively affected during times of peak hypersalinity (Nübel *et al.*, 2000; Abed *et al.*, 2007). This negative effect of hypersalinity has previously been shown to occur in the microbial mats of SL (Pinckney *et al.*, 1995). Only the shallower calcareous knob in SL showed any appreciable cyanobacterial population in our study ($\sim 3\%$), while cyanobacteria were almost negligible in the deeper cheesecake, cauliflower-top mushroom, and pinnacle mound mats. In contrast, anaerobic photosynthesizers of the phylum Chloroflexi (*e.g.*, green nonsulfur bacteria) were identified even in these deeper mats in spite of the low amounts of sunlight received at these depths.

The dissolved oxygen content at the deeper sections of the lake was low, thus potentially promoting the growth of anoxygenic phototrophic bacteria, even under limited light conditions. Members of purple sulfur bacteria of the class Gammaproteobacteria, which were prevalent in the shallow calcareous knobs, can oxidize hydrogen sulfide produced by SRB (important members of Deltaproteobacteria) and, in turn, provide sulfate for use by SRB. The presence of these phototrophs is indicative that light, albeit in low amounts, reached the lake bottom with enough intensity to stimulate their metabolic activity. These organisms can oxidize sulfides produced by SRB respiration, thus cycling sulfur and carbon within the microbial mat system. Fermenters, such as members of the class Phycisphaerae (maximum of 7% in the cheesecake microbial mat) and phyla Spirochaetes were also present in the SL microbial mats, indicating the metabolically diverse population present (Magot *et al.*, 1997; Fukunaga *et al.*, 2009; Dubinina *et al.*, 2011; Lee *et al.*, 2014).

4.4. Microbial influence on carbonate mineral precipitation and lithification

The results from the microscopic investigations of the microbial mat in the plateau-mushroom microbialite and the water column reveal that at least some carbonate particles in the suspended water column could settle on the microbialite surface. However, this finding does not rule out the *in situ* carbonate biomineralization (by the microorganisms) and/or organo-mineralization (the influence of organic matrix, EPS, etc.) in the microbial mats. Another line of evidence for the occurrence of biomineralization can be gathered from the preferred orientation of the crystals of acicular aragonite (Fig. 8A), indicating that the minerals were precipitated by microbial activity (Weiner and Dove, 2003).

The microbialites at the deeper locations in SL have been suggested to be inactive or ''sub-fossilized'' (Dupraz *et al.*, 2006, 2013; Fowler, 2011). However, carbonate mineral–precipitating microbial communities, including anaerobic phototrophs and sulfate reducers (except for cyanobacteria), were detected in all mats sampled (Fig. 9B), although it was not clear whether these microorganisms are actively contributing to the precipitation on the microbialite head. In the absence of cyanobacteria, carbonate mineralization can still potentially occur with the activity of SRB and anoxygenic phototrophs (Visscher *et al.*, 2000; Dupraz and Visscher, 2005). Considering the possibility that only shallow-water calcareous knob microbialites are the ''actively'' forming microbialites, the SRB families in class Deltaproteobacteria ($\sim 18\%$) were present in higher number than the phylum Cyanobacteria ($\sim 3.2\%$) in these mats. This large representation of Deltaproteobacteria indicates that the SRB are likely playing an active role in carbonate mineral precipitation (Nitti *et al.*, 2012). As the SRB and anoxygenic phototrophs were present in significant percentages in all mat types, it is possible that these two groups influence carbonate mineralization in SL. The role of SRB in the precipitation of carbonate minerals in microbialites has been verified by using the $^{35}SO_4^{2-}$ coated Ag-foil technique, where maximum SRB activity has been shown to precipitate a calcified laminae (Visscher *et al.*, 2000). Studies on the role of anoxygenic phototrophs on carbonate precipitation have been gaining more attention (Bundeleva *et al.*, 2012; Nitti *et al.*, 2012), and this investigation further helps strengthen the importance of this microbial group as a key member in a microbialite mat community. It is important to note that, in addition to the abundance or even presence of microorganisms capable of carbonate mineral precipitation, knowledge of their metabolic rates and the gene expression pattern over spatial and temporal extent in the microbial mat is essential to better understand the actual mechanisms involved (Dupraz and Visscher, 2005).

Storr's Lake microbialites reveal that a microbial community with a significant lack of cyanobacteria can still be involved in the precipitation of carbonate minerals. We show here that sulfate reducers and anoxygenic phototrophs, as part of the microbial mat community, could be capable of sustaining carbonate mineral precipitation and the related growth that occurs in a microbialite. This understanding widens the ecology and associated metabolic functioning of various microbial communities within the mat that contributed to the formation of ancient microbialites. For example, in an ancient environment with limited oxygen in the ocean and atmosphere, anoxygenic phototrophs and sulfate reducers could have been key members in a microbialite community. Our study further highlights the complexity of the microbial mat system in the SL environment, where several biogeochemical components are suspected to play an interactive role in the precipitation and lithification of the microbialites.

5. Conclusions

Our research builds upon previous analysis and interpretation of (i) the water parameters, (ii) microbialite distribution and mineralogy, and (iii) the microbial mat composition through the application of molecular tools. Light-penetration studies revealed that the turbid water restricted >97% of the luminosity to the deeper sections of the lake. One of our main findings was the identification of aragonite as a significant part of the microbialite mineralogical composition in the plateau-mushroom and pinnacle mound microbialites. Secondly, a new microbialite morphology, ''multi-cuspate,'' was discovered near Cactus Island and categorized as a subfossil because of the lack of prominent microbial mat on its surface. Thirdly, our molecular diversity analysis of the microbial mats, the major focus of this investigation, revealed that the cyanobacterial population was generally low and almost negligible in certain deeper-water microbial mats. The lack of prominent cyanobacterial populations can be explained by the less intense sunlight reaching those depths. On the other hand, a plethora of anaerobic phototrophs exist in these deeper water mats, indicating that factors such as oxygen availability or the lack of it is controlling the distribution of these phototrophs in the dim-light conditions under which they exist. Though most reported microbialite communities are typically found in clear waters, the SL microbialites present an anomaly to this view as they exist under highly turbid and light-limiting conditions. Hence, these and other uncommon examples further necessitate the exploration of potential unique and diverse environments in which microbialites could be found. Investigations on SL microbialites have potential implications for understanding possible life on other planets and in applied areas, such as carbon sequestration, where microbial activity could enhance the conversion of CO_2 gas into carbonate minerals in the absence of light. A better knowledge of such microbialite systems could also provide useful clues with regard to past climatic and environmental conditions and act as a possible indicator of local or global climate in the future.

Acknowledgments

Funding for this study was provided by the Department of Energy–National Energy Technology Lab under agreement DE-FE0002416. Travel expenses were partially covered by Donald Radcliffe Trust–Geology and Geophysics Department, Missouri S&T. We thank the staff of the Gerace Research Centre, San Salvador Island, for providing logistics, transportation and laboratory access while we were stationed on the island, and the Bahamas Environment Science & Technology Commission (BEST) for permission to sample and export microbialite samples. We also thank the Advanced Material Characterization Laboratory (AMCL), Materials Research Center (MRC), and Environmental Research Center (ERC) at Missouri S&T for access to SEM, XRD, and ICP-OES instrumentation, respectively. We thank Joshua Silverstein and Carlos Sanchez (Missouri S&T) for help with XRD sample preparation and optical microscopy, respectively. We also thank Shreya Ghosh (Missouri S&T) for her insightful discussions on the use of QIIME for our bioinformatics analyses.

Author Disclosure Statement

No competing financial interests exist.

References

Abed, R.M., Kohls, K., and de Beer, D. (2007) Effect of salinity changes on the bacterial diversity, photosynthesis and oxygen consumption of cyanobacterial mats from an intertidal flat of the Arabian Gulf. *Environ Microbiol* 9:1384–1392.

Al-Najjar, M.A., de Beer, D., Kühl, M., and Polerecky, L. (2012) Light utilization efficiency in photosynthetic microbial mats. *Environ Microbiol* 14:982–992.

Bailey, J.V., Orphan, V.J., Joye, S.B., and Corsetti, F.A. (2009) Chemotrophic microbial mats and their potential for preservation in the rock record. *Astrobiology* 9:843–859.

Boyd, C.E. (2002, February) Specific conductance, alternative salinity measurement. *The Advocate* 70–71.

Braissant, O., Decho, A.W., Dupraz, C., Glunk, C., Przekop, K.M., and Visscher, P.T. (2007) Exopolymeric substances of sulfate-reducing bacteria: interactions with calcium at alkaline pH and implication for formation of carbonate minerals. *Geobiology* 5:401–411.

Breitbart, M., Hoare, A., Nitti, A., Siefert, J., Haynes, M., Dinsdale, E., Edwards, R., Souza, V., Rohwer, F., and Hollander, D. (2009) Metagenomic and stable isotopic analyses of modern freshwater microbialites in Cuatro Cienegas, Mexico. *Environ Microbiol* 11:16–34.

Brigmon, R.L., Smith, G., Morris, P., Byrne, M., and McKay, D. (2006) Microbial ecology in modern stromatolites from San Salvador, Bahamas. In *Proceedings of the Twelfth Symposium on the Geology of the Bahamas and Other Carbonate Regions*, edited by R.L. Davis and D.W. Gamble, Gerace Research Centre, San Salvador, Bahamas, pp 1–12.

Bundeleva, I.A., Shirokova, L.S., Bénézeth, P., Pokrovsky, O.S., Kompantseva, E.I., and Balor, S. (2012) Calcium carbonate precipitation by anoxygenic phototrophic bacteria. *Chem Geol* 291:116–131.

Burne, R.V. and Moore, L.S. (1987) Microbialites: organosedimentary deposits of benthic microbial communities. *Palaios* 2:241–254.

Caporaso, J.G., Kuczynski, J., Stombaugh, J., Bittinger, K., Bushman, F.D., Costello, E.K., Fierer, N., Pena, A.G., Goodrich, J.K., and Gordon, J.I. (2010) QIIME allows analysis of high-throughput community sequencing data. *Nat Methods* 7:335–336.

Castenholz, R.W. and García-Pichel, F. (2000) Cyanobacterial responses to UV-radiation. In *The Ecology of Cyanobacteria: Their Diversity in Time and Space*, edited by B.A. Whitton and M. Potts, Kluwer, Dordrecht, pp 591–611.

Decho, A.W., Visscher, P.T., and Reid, R.P. (2005) Production and cycling of natural microbial exopolymers (EPS) within a marine stromatolite. *Palaeogeogr Palaeoclimatol Palaeoecol* 219:71–86.

DeSantis, T.Z., Hugenholtz, P., Larsen, N., Rojas, M., Brodie, E.L., Keller, K., Huber, T., Dalevi, D., Hu, P., and Andersen, G.L. (2006) Greengenes, a chimera-checked 16S rRNA gene database and workbench compatible with ARB. *Appl Environ Microbiol* 72:5069–5072.

Dojka, M.A., Hugenholtz, P., Haack, S.K., and Pace, N.R. (1998) Microbial diversity in a hydrocarbon-and chlorinated-solvent-contaminated aquifer undergoing intrinsic bioremediation. *Appl Environ Microbiol* 64:3869–3877.

Dubinina, G., Grabovich, M., Leshcheva, N., Rainey, F.A., and Gavrish, E. (2011) *Spirochaeta perfilievii* sp. nov., an oxygen-tolerant, sulfide-oxidizing, sulfur-and thiosulfate-reducing spirochaete isolated from a saline spring. *Int J Syst Evol Microbiol* 61:110–117.

Dupraz, C. and Visscher, P.T. (2005) Microbial lithification in marine stromatolites and hypersaline mats. *Trends Microbiol* 13:429–438.

Dupraz, C., Visscher, P.T., Baumgartner, L., and Reid, R. (2004) Microbe-mineral interactions: early carbonate precipitation in a hypersaline lake (Eleuthera Island, Bahamas). *Sedimentology* 51:745–765.

Dupraz, C., Pattisina, R., and Verrecchia, E.P. (2006) Translation of energy into morphology: simulation of stromatolite morphospace using a stochastic model. *Sediment Geol* 185:185–203.

Dupraz, C., Reid, R.P., Braissant, O., Decho, A.W., Norman, R.S., and Visscher, P.T. (2009) Processes of carbonate precipitation in modern microbial mats. *Earth-Science Reviews* 96:141–162.

Dupraz, C., Fowler, A., Tobias, C., and Visscher, P.T. (2013) Stromatolitic knobs in Storr's Lake (San Salvador, Bahamas): a model system for formation and alteration of laminae. *Geobiology* 11:527–548.

Ferris, F.G., Thompson, J.B., and Beveridge, T.J. (1997) Modern freshwater microbialites from Kelly Lake, British Columbia, Canada. *Palaios* 12:213–219.

Fowler, A.J. (2011) Stromatolitic knobs in Storr's Lake, San Salvador, Bahamas: insights into organomineralization. Master's thesis, University of Connecticut, Storrs, CT.

Freytet, P. and Verrecchia, E.P. (1998) Freshwater organisms that build stromatolites: a synopsis of biocrystallization by prokaryotic and eukaryotic algae. *Sedimentology* 45:535–563.

Frigaard, N.U. and Bryant, D.A. (2004) Seeing green bacteria in a new light: genomics-enabled studies of the photosynthetic apparatus in green sulfur bacteria and filamentous anoxygenic phototrophic bacteria. *Arch Microbiol* 182:265–276.

Fukunaga, Y., Kurahashi, M., Sakiyama, Y., Ohuchi, M., Yokota, A., and Harayama, S. (2009) *Phycisphaera mikurensis* gen. nov., sp. nov., isolated from a marine alga, and proposal of Phycisphaeraceae fam. nov., Phycisphaerales ord. nov. and Phycisphaerae classis nov. in the phylum Planctomycetes. *J Gen Appl Microbiol* 55:267–275.

Furman, F.C., Woody, R.E., Rasberry, M.A., Keller, D.J., and Gregg, J.M. (1993) Carbonate and evaporite mineralogy of Holocene (<1900 RCYBP) sediments at Salt Pond, San Salvador Island, Bahamas: preliminary study. In *Proceedings of the Sixth Symposium on the Geology of the Bahamas*, edited by B.N. White, Bahamian Field Station, San Salvador, Bahamas, pp 47–54.

Garrett, P. (1970) Phanerozoic stromatolites: noncompetitive ecologic restriction by grazing and burrowing animals. *Science* 169:171–173.

Glunk, C., Dupraz, C., Braissant, O., Gallagher, K.L., Verrecchia, E.P., and Visscher, P.T. (2011) Microbially mediated carbonate precipitation in a hypersaline lake, Big Pond (Eleuthera, Bahamas). *Sedimentology* 58:720–736.

Green, S.J., Blackford, C., Bucki, P., Jahnke, L.L., and Prufert-Bebout, L. (2008) A salinity and sulfate manipulation of hypersaline microbial mats reveals stasis in the cyanobacterial community structure. *ISME J* 2:457–470.

Haas, B.J., Gevers, D., Earl, A.M., Feldgarden, M., Ward, D.V., Giannoukos, G., Ciulla, D., Tabbaa, D., Highlander, S.K., Sodergren, E., Methe, B., DeSantis, T.Z., Human Microbiome Consortium, Petrosino, J.F., Knight, R., and Birren, B.W. (2011) Chimeric 16S rRNA sequence formation and detection in Sanger and 454-pyrosequenced PCR amplicons. *Genome Res* 21:494–504.

Hattin, D.E. (1983) Holocene lithification of carbonate sediments San Salvador Island, Bahamas. In *Proceedings of the First Symposium on the Geology of the Bahamas*, College Center of the Finger Lakes, Bahamian Field Station, San Salvador, Bahamas, pp 41–51.

Hofmann, H., Grey, K., Hickman, A., and Thorpe, R. (1999) Origin of 3.45 Ga coniform stromatolites in Warrawoona Group, Western Australia. *Geol Soc Am Bull* 111:1256–1262.

Hugenholtz, P., Pitulle, C., Hershberger, K.L., and Pace, N.R. (1998) Novel division level bacterial diversity in a Yellowstone hot spring. *J Bacteriol* 180:366–376.

Imhoff, J. (2006) The Chromatiaceae. In *The Prokaryotes*, Vol. 6, 3rd ed., edited by M. Dworkin, S. Falkow, E. Rosenberg, K.-H. Schleifer, and E. Stackebrandt, Springer-Verlag, New York, pp 846–873.

Jones, B., Renaut, R.W., and Rosen, M.R. (1998) Microbial biofacies in hot-spring sinters; a model based on Ohaaki Pool, North Island, New Zealand. *Journal of Sedimentary Research* 68:413–434.

Jørgensen, B., Cohen, Y., and Des Marais, D. (1987) Photosynthetic action spectra and adaptation to spectral light distribution in a benthic cyanobacterial mat. *Appl Environ Microbiol* 53:879–886.

Krauskopf, K.B. and Bird, D.K. (1994) *Introduction to Geochemistry*, 3rd ed., McGraw-Hill, New York.

Kühl, M., Chen, M., Ralph, P.J., Schreiber, U., and Larkum, A.W. (2005) Ecology: a niche for cyanobacteria containing chlorophyll *d*. *Nature* 433:820.

Laval, B., Cady, S.L., Pollack, J.C., McKay, C.P., Bird, J.S., Grotzinger, J.P., Ford, D.C., and Bohm, H.R. (2000) Modern freshwater microbialite analogues for ancient dendritic reef structures. *Nature* 407:626–629.

Lee, J.Z., Burow, L.C., Woebken, D., Everroad, R.C., Kubo, M.D., Spormann, A.M., Weber, P.K., Pett-Ridge, J., Bebout, B.M., and Hoehler, T.M. (2014) Fermentation couples Chloroflexi and sulfate-reducing bacteria to Cyanobacteria in hypersaline microbial mats. *Front Microbiol* 5:1–17.

Ley, R.E., Harris, J.K., Wilcox, J., Spear, J.R., Miller, S.R., Bebout, B.M., Maresca, J.A., Bryant, D.A., Sogin, M.L., and Pace, N.R. (2006) Unexpected diversity and complexity of the Guerrero Negro hypersaline microbial mat. *Appl Environ Microbiol* 72:3685–3695.

Lim, D.S., Laval, B.E., Slater, G., Antoniades, D., Forrest, A.L., Pike, W., Pieters, R., Saffari, M., Reid, D., Schulze-Makuch, D., Andersen, D., and McKay, C.P. (2009) Limnology of Pavilion Lake, BC, Canada—characterization of a microbialite forming environment. *Fundamental and Applied Limnology/Archiv für Hydrobiologie* 173:329–351.

Lösekann, T., Knittel, K., Nadalig, T., Fuchs, B., Niemann, H., Boetius, A., and Amann, R. (2007) Diversity and abundance of aerobic and anaerobic methane oxidizers at the Haakon Mosby Mud Volcano, Barents Sea. *Appl Environ Microbiol* 73:3348–3362.

Lozupone, C. and Knight, R. (2005) UniFrac: a new phylogenetic method for comparing microbial communities. *Appl Environ Microbiol* 71:8228–8235.

Magot, M., Fardeau, M.L., Arnauld, O., Lanau, C., Ollivier, B., Thomas, P., and Patel, B. (1997) *Spirochaeta smaragdinae* sp. nov., a new mesophilic strictly anaerobic spirochete from an oil field. *FEMS Microbiol Lett* 155:185–191.

Mann, C.J. and Nelson, W.M. (1989) Microbialitic structures in Storr's lake, San Salvador Island, Bahama Islands. *Palaios* 4:287–293.

Marcarelli, A.M., Wurtsbaugh, W.A., and Griset, O. (2006) Salinity controls phytoplankton response to nutrient enrichment in the Great Salt Lake, Utah, USA. *Can J Fish Aquat Sci* 63:2236–2248.

Muyzer, G., de Waal, E.C., and Uitterlinden, A.G. (1993) Profiling of complex microbial populations by denaturing gradient gel electrophoresis analysis of polymerase chain reaction-amplified genes coding for 16S rRNA. *Appl Environ Microbiol* 59:695–700.

Neumann, C., Bebout, B., McNeese, L., Paull, C., and Paerl, H. (1989) Modern stromatolites and associated mats: San Salvador, Bahamas. In *Proceedings of the Fourth Symposium on the Geology of the Bahamas*, edited by J.E. Mylroie, Bahamian Field Station, San Salvador, Bahamas, pp 243–254.

Nitti, A., Daniels, C.A., Siefert, J., Souza, V., Hollander, D., and Breitbart, M. (2012) Spatially resolved genomic, stable isotopic, and lipid analyses of a modern freshwater microbialite from Cuatro Ciénegas, Mexico. *Astrobiology* 12:685–698.

Nübel, U., García-Pichel, F., Clavero, E., and Muyzer, G. (2000) Matching molecular diversity and ecophysiology of benthic cyanobacteria and diatoms in communities along a salinity gradient. *Environ Microbiol* 2:217–226.

Oren, A. and Rodríguez-Valera, F. (2001) The contribution of halophilic bacteria to the red coloration of saltern crystallizer ponds (1). *FEMS Microbiol Ecol* 36:123–130.

Paerl, H.W., Steppe, T.F., Buchan, K.C., and Potts, M. (2003) Hypersaline cyanobacterial mats as indicators of elevated tropical hurricane activity and associated climate change. *AMBIO: A Journal of the Human Environment* 32:87–90.

Park, L.E. (2012) Comparing two long-term hurricane frequency and intensity records from San Salvador Island, Bahamas. *Journal of Coastal Research* 28:891–902.

Paull, C., Neumann, A., Bebout, B., Zabielski, V., and Showers, W. (1992) Growth rate and stable isotopic character of modern stromatolites from San Salvador, Bahamas. *Palaeogeogr Palaeoclimatol Palaeoecol* 95:335–344.

Pentecost, A. (1989) Observations on the *Scytonema* mats of San Salvador, Bahamas. In *Proceedings of the Fourth Symposium on the Geology of the Bahamas*, edited by J.E. Mylroie, Bahamian Field Station, San Salvador, Bahamas, pp 295–302.

Pinckney, J., Paerl, H., and Bebout, B. (1995) Salinity control of benthic microbial mat community production in a Bahamian hypersaline lagoon. *J Exp Mar Bio Ecol* 187:223–237.

Reid, R.P., Visscher, P.T., Decho, A.W., Stolz, J.F., Bebout, B., Dupraz, C., Macintyre, I., Paerl, H., Pinckney, J., and Prufert-Bebout, L. (2000) The role of microbes in accretion, lamination and early lithification of modern marine stromatolites. *Nature* 406:989–992.

Riding, R. (1991) *Calcareous Algae and Stromatolites*, Springer-Verlag, Berlin.

Riding, R. (2000) Microbial carbonates: the geological record of calcified bacterial-algal mats and biofilms. *Sedimentology* 47:179–214.

Saini-Eidukat, B. and Yahin, A. (1999) Web-PHREEQ: a WWW instructional tool for modeling the distribution of chemical species in water. *Comput Geosci* 25:347–353.

Skyring, G. and Bauld, J. (1990) Microbial mats in Australian coastal environments. *Adv Microb Ecol* 11:461–498.

Sommers, M., Awramik, S., and Woo, K. (2000) Evidence for initial calcite-aragonite composition of Lower Algal Chert Member ooids and stromatolites, Paleoproterozoic Gunflint Formation, Ontario, Canada. *Can J Earth Sci* 37:1229–1243.

Van Gemerden, H. (1993) Microbial mats: a joint venture. *Mar Geol* 113:3–25.

Vasconcelos, C. and McKenzie, J.A. (1997) Microbial mediation of modern dolomite precipitation and diagenesis under anoxic conditions (Lagoa Vermelha, Rio de Janeiro, Brazil). *Journal of Sedimentary Research* 67:378–390.

Visscher, P.T. and Stolz, J.F. (2005) Microbial mats as bioreactors: populations, processes, and products. *Palaeogeogr Palaeoclimatol Palaeoecol* 219:87–100.

Visscher, P.T., Reid, R.P., Bebout, B.M., Hoeft, S.E., Macintyre, I.G., and Thompson, J.A. (1998) Formation of lithified micritic laminae in modern marine stromatolites (Bahamas): the role of sulfur cycling. *Am Mineral* 83:1482–1493.

Visscher, P.T., Reid, R.P., and Bebout, B.M. (2000) Microscale observations of sulfate reduction: correlation of microbial activity with lithified micritic laminae in modern marine stromatolites. *Geology* 28:919–922.

Weiner, S. and Dove, P.M. (2003) An overview of biomineralization processes and the problem of the vital effect. *Reviews in Mineralogy and Geochemistry* 54:1–29.

Weisburg, W.G., Barns, S.M., Pelletier, D.A., and Lane, D.J. (1991) 16S ribosomal DNA amplification for phylogenetic study. *J Bacteriol* 173:697–703.

Zabielski, V.P. (1991) The depositional history of Storr's Lake San Salvador Island, Bahamas. PhD dissertation, University of North Carolina at Chapel Hill, Chapel Hill, NC.

Address correspondence to:
Varun G. Paul
Department of Geological Sciences
Missouri University of Science and Technology
146 McNutt Hall
Rolla, MO 65409

E-mail: varungpaul@gmail.com

Submitted 26 March 2015
Accepted 26 November 2015

Abbreviations Used

EPS	= exopolymeric substances
GRC	= Gerace Research Centre
ICP-OES	= inductively coupled plasma–optical emission spectrometry
Missouri S&T	= Missouri University of Science and Technology
NTU	= nephelometric turbidity units
OTUs	= operational taxonomic units
PCR	= polymerase chain reaction
PM	= pinnacle mound
SEM-EDS	= scanning electron microscopy–energy dispersive spectroscopy
SI	= saturation index
SL	= Storr's Lake
SRB	= sulfate-reducing bacteria
UPGMA	= unweighted pair group method with arithmetic mean
XRD	= X-ray diffraction